

Award Accounts

The Chemical Society of Japan Award for Young Chemists for 2007

Development of a New System for Photocatalytic Water Splitting into H_2 and O_2 under Visible Light Irradiation

Ryu Abe

Catalysis Research Center, Hokkaido University, North 21, West 10, Kita-ku, Sapporo 001-0021

Received May 9, 2011; E-mail: ryu-abe@cat.hokudai.ac.jp

Photocatalytic water splitting using semiconductor materials has attracted considerable interest due to its potential for clean production of H_2 from water by utilizing abundant solar light. The developments of water-splitting systems that can efficiently use visible light have been a major challenge for many years in order to realize efficient conversion of solar light. We have developed a new type of photocatalysis system that can split water into H_2 and O_2 under visible light irradiation, which was inspired by the two-step photoexcitation (Z-scheme) mechanism of natural photosynthesis in green plants. In this system, the water-splitting reaction is broken up into two stages: one for H_2 evolution and the other for O_2 evolution; these are combined by using a shuttle redox couple (Red/Ox) in the solution. The introduction of a Z-scheme mechanism reduces the energy required to drive each photocatalysis process, extending the usable wavelengths significantly (≈660 nm for H_2 evolution and ≈600 nm for O_2 evolution) from that in conventional water splitting systems (≈460 nm) based on one-step photoexcitation in single semiconductor material.

1. Introduction

1.1 Production of H_2 from Water Using Solar Radiation. A great technological challenge is the development of a clean and renewable energy carrier that does not utilize fossil fuels. One of the most attractive proposals is the large-scale utilization of hydrogen (H_2) as a recyclable energy carrier. However, industrial H_2 production consumes huge amounts of fossil fuels (e.g., natural gas), resulting in equally large amounts of CO_2 being released. Photocatalytic and photoelectrochemical water splitting using semiconductor materials has thus attracted considerable interest due to its potential for clean production of H_2 from water by utilizing abundant solar light. Ever since Fujishima and Honda reported photoelectrochemical water splitting using a TiO_2 electrode in 1972,[1] numerous researchers have intensively studied water splitting using semiconductor photoelectrodes or photocatalysts.[2–7] In such systems, light energy is converted into chemical energy and the Gibbs free energy increases greatly by the following water-splitting reaction:

$$H_2O + h\nu \rightarrow H_2 + 1/2O_2 \quad \Delta G^\circ = 238\,\mathrm{kJ\,mol^{-1}} \quad (1)$$

Since photocatalytic or photoelectrochemical water splitting resembles photosynthesis in green plants it is regarded as being a form of artificial photosynthesis. Heterogeneous photocatalytic systems that use semiconductor powders have several advantages over photoelectrochemical systems, including greater simplicity and lower cost. Consequently, extensive efforts have been made to develop efficient heterogeneous photocatalysts by investigating new semiconductor materials. Although more than 100 photocatalytic systems based on metal oxides have been reported to be active for "overall" water splitting (i.e., simultaneous generation of both H_2 and O_2), most of them function only under ultraviolet (UV) light ($\lambda < 400$ nm) because of the large band-gap energy of semiconductor materials.[8–73] Since nearly half of the solar energy incident on the Earth's surface lies in the visible region ($400 < \lambda < 800$ nm) (Figure 1), it is essential to use visible light efficiently to realize practical H_2 production on a huge scale by photocatalytic water splitting. The maximum solar conversion efficiency for photocatalytic water splitting with a quantum efficiency of 100% can be calculated using the standard solar spectrum. Even if all UV light up to 400 nm were utilized, the solar conversion efficiency would be only 2%, which is similar to the maximum conversion efficiencies of photosynthesis in green plants under normal environmental conditions (1–2%).[74] However, the utilization of visible light up to 600 nm can drastically improve the efficiency to 16%; a further extension up to 800 nm would give a conversion efficiency of 32%. Therefore, achieving water splitting under visible light has been a challenging goal since the discovery of the Honda–Fujishima effect in 1972. Despite many years of intensive effort by researchers around the world, the first reproducible demonstration of water splitting under visible light was reported only a decade ago. The first demonstration of visible-light-driven water splitting,[75–77] which was inspired by photosynthesis in nature, is reviewed in Section **3**.

Published on the web September 27, 2011; doi:10.1246/bcsj.20110132

1.2 Difficulties in Achieving Water Splitting under Visible Light Using Heterogeneous Semiconductor Photocatalysts. Figure 2 shows a schematic diagram of water splitting into H_2 and O_2 over a heterogeneous semiconductor photocatalyst. Photocatalysis on semiconductor particles involves three main steps: (i) absorption of photons with higher energies than the semiconductor band gap, leading to the generation of electron (e^-)–hole (h^+) pairs in the semiconductor particles; (ii) charge separation followed by migration of these photogenerated carriers in the semiconductor particles; (iii) surface chemical reactions between these carriers with various compounds (e.g., H_2O); electrons and holes may also recombine with each other without participating in any chemical reactions. When a heterogeneous semiconductor photocatalyst is used for water splitting, the bottom of the conduction band must be more negative than the reduction potential of water to produce H_2, and the top of the valence band must be more positive than the oxidation potential of water to produce O_2 (Figure 3a). Furthermore, the photocatalyst must be stable in aqueous solutions under photoirradiation. Oxide semiconductors are generally highly stable against photocorrosion and have thus been extensively used as heterogeneous photocatalysts. However, Scaife noted in 1980 that it is intrinsically difficult to develop an oxide semiconductor photocatalyst that has both a sufficiently negative conduction band for H_2 production and a sufficiently narrow band gap (i.e., <3.0 eV) for visible light absorption because of the highly positive valence band (at ca. +3.0 V vs. NHE) formed by the O 2p orbital.[78] Indeed, most visible-light-responsive oxide photocatalysts, such as tungsten oxide (WO_3)[79–81] or bismuth vanadate ($BiVO_4$),[82–85] cannot produce H_2 from water due to their conduction bands being too low for water reduction (Figure 3b). Although some non-oxide semiconductors, such as sulfides[86–91] and nitrides,[92,93] posses appropriate band levels for water splitting under visible light (Figure 3c), they are generally unstable and readily become deactivated through photocorrosion or self-oxidation, rather than evolving O_2. For example, cadmium sulfide CdS has appropriate band levels for water reduction and oxidation as well as a narrow band gap that permits visible light absorption. Indeed, CdS particles loaded with a cocatalyst such as Pt exhibit a high H_2 production activity under visible light irradiation in the presence of a sacrificial electron donor such as Na_2SO_3.[86,94–97] However, S^{2-} anions in the CdS semiconductor are preferentially oxidized over H_2O molecules by photogenerated holes in the absence of a sacrificial electron donor.

Another class of non-oxide semiconductor photocatalyst is homogeneous sensitizer molecules, such as organic dyes and metal complexes.[98–116] As a strategy for achieving effective visible light harvesting, spectral sensitization of wide-band-gap semiconductors (e.g., TiO_2) by such sensitizer molecules has been studied for photocatalytic H_2 production from water. The

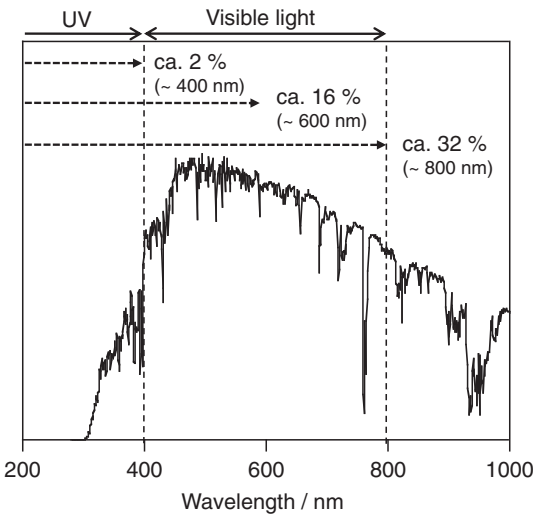

Figure 1. Solar spectrum and maximum solar light conversion efficiencies for water-splitting reaction with 100% of quantum efficiency.

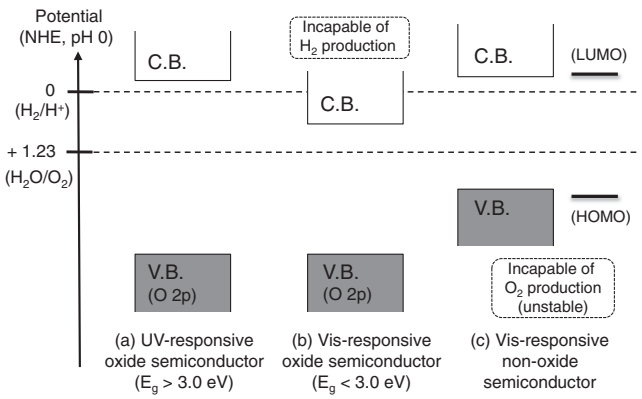

Figure 3. Band energy levels of various semiconductors.

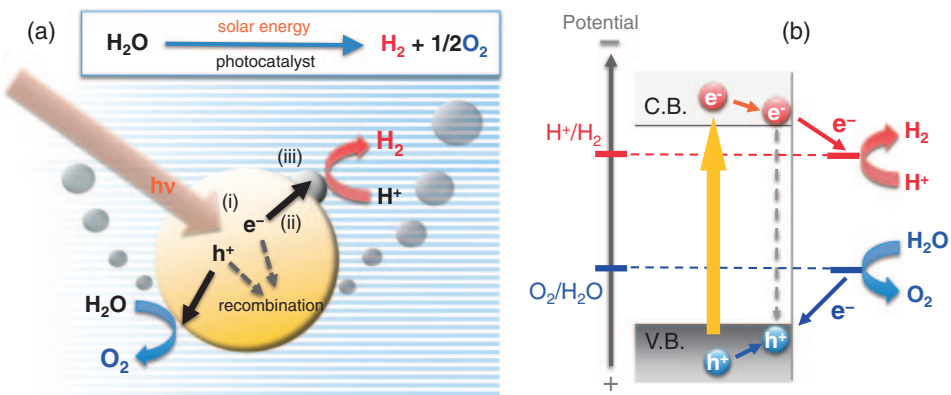

Figure 2. Schematic illustration of water splitting over semiconductor photocatalyst.

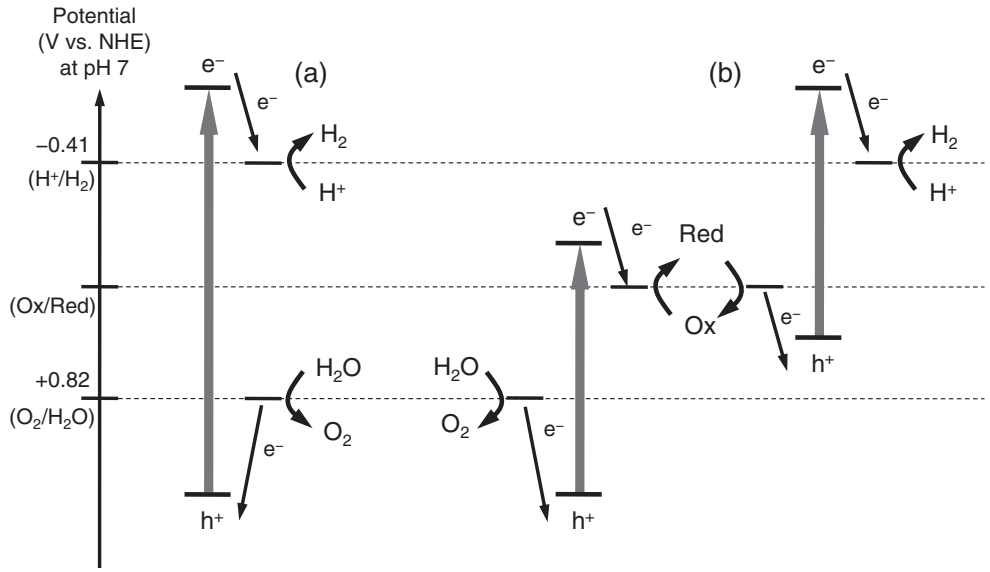

Figure 4. Schematic energy diagrams of photocatalytic water-splitting systems: (a) conventional one-step system and (b) two-step photoexcitation system.

adsorption of molecular sensitizers such as $[Ru(bpy)_3]^{2+}$ or Eosin Y on platinized titanium oxide (Pt/TiO_2) particles resulted in efficient H_2 evolution from water under visible light irradiation in the presence of a sacrificial electron donor such as triethanolamine or ethylenediaminetetraacetic acid.[98–108] However, the sensitizer molecules themselves cannot oxidize H_2O to O_2 and they generally decompose through self-oxidation under photoirradiation in the absence of a sacrificial electron donor. Because the evolution of O_2 from water requires the abstraction of four electrons, it is quite difficult for it to occur on simple sensitizer molecules, in which only one positive or negative charge can be stored. Only a few studies have achieved appreciable O_2 generation from water using a Ru complex combined with a colloidal hydrated iridium oxide ($IrO_2 \cdot nH_2O$)[114,115] or a molecular manganese complex,[116] which can scavenge the positive charge in the Ru complex and acts as catalyst for O_2 evolution. As mentioned above, there are not many stable semiconductors that have both a sufficient visible light absorption and a sufficiently high potential for water splitting. Thus, achieving water splitting using heterogeneous photocatalysts under visible light has been a major challenge for many years.

1.3 Two Strategies for Achieving Water Splitting Using Heterogeneous Photocatalysts under Visible Light. There are two main approaches for achieving water splitting using visible light. One approach is to split water into H_2 and O_2 using a single visible-light-responsive photocatalyst (a one-step system), as illustrated in Figure 4a. Because there are few stable semiconductors that can absorb visible light and have a sufficiently high potential for water splitting, band engineering of semiconductors is required to artificially develop new photocatalyst materials that satisfy the following requirements for water splitting under visible light: (i) have a narrow band gap, (ii) are stable under photoirradiation, and (iii) have suitable conduction and valence band levels for H_2 and O_2 production. Various band-engineering methods have been studied, including introduction of a midgap electron donor level (doped materials),[117–126] hybridization of the O 2p orbital with other orbitals (oxides,[83,127–131] oxynitrides,[92,132–137] and oxysulfides[138–141]), and the formation of solid solutions.[142–147] However, there are still few reliable photocatalysts for one-step water splitting under visible light due to the stringent requirements.[142–144] An effective one-step water-splitting system that uses a solid solution photocatalyst such as $(Ga_{1-x}Zn_x)(N_{1-x}O_x)$ or $(Zn_{1+x}Ge)(N_2O_x)$ has been developed by Domen et al., while the usable wavelength is still limited to under 460 nm.[142–144]

The other approach for achieving water splitting using visible light is to apply a two-step photoexcitation mechanism between two different photocatalysts (a two-step system; Figure 4b).[75–77,113,148–160] This process was inspired by natural photosynthesis in green plants and is known as the Z-scheme. In two-step systems, the water-splitting reaction is broken up into two stages: one for H_2 evolution and the other for O_2 evolution; these are combined by using a shuttle redox couple (Red/Ox) in the solution. Over a H_2 evolution photocatalyst, the photoexcited electrons reduce water to H_2 and holes in the valence band oxidize the reductant (Red) to an oxidant (Ox). The oxidant is reduced back to the reductant by photoexcited electrons generated over an O_2 evolution photocatalyst, where the holes oxidize water to O_2. This system lowers the energy required for photocatalysis, allowing visible light to be utilized more efficiently than in conventional water-splitting systems (Figure 4a). In other words, it enables a semiconductor to be used that has a water reduction or oxidation potential suitable for one side of the system. For example, visible-light-responsive oxides such as WO_3 can be used as O_2 evolution photocatalysts if they can reduce the oxidant to a reductant. Similarly, non-oxide photocatalysts (e.g., sulfides, oxynitrides, and dyes) can be used as H_2 evolution photocatalysts if they can oxidize the reductant to an oxidant. Consequently, various semiconductor materials can be used in the Z-scheme even if they do not satisfy all the stringent requirements for a one-step system. Another advantage of Z-scheme systems is the ability to separate production of H_2 and O_2 by employing a separator

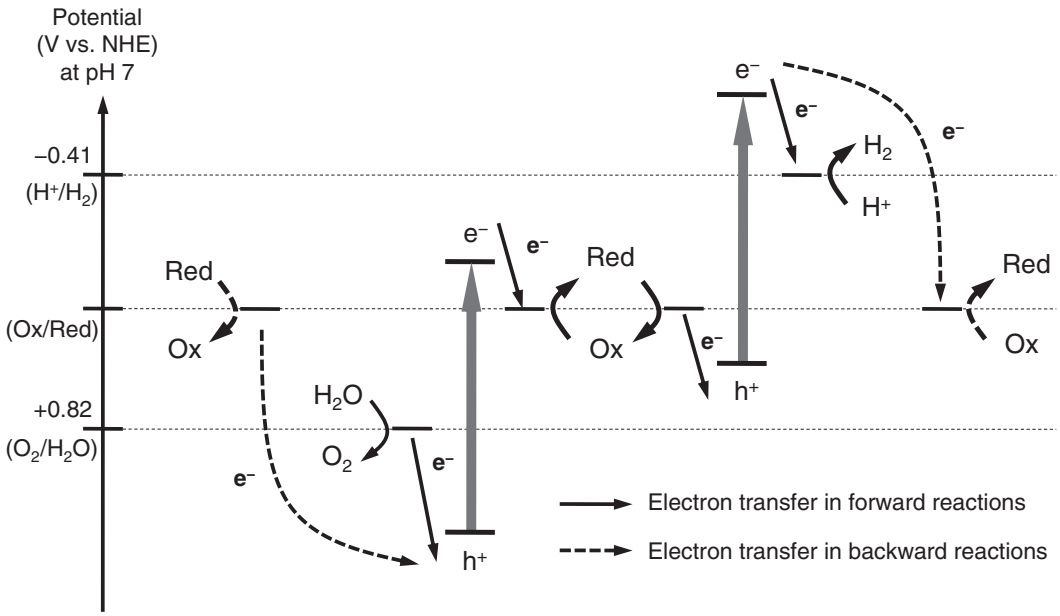

Figure 5. Forward and backward reactions in the two-step photoexcitation system.

that permits only redox mediators to be transferred. It is impossible in principle to achieve separate production of H_2 and O_2 in a conventional one-step water-splitting system since H_2 and O_2 are evolved simultaneously on small semiconductor particles.

1.4 Difficulties in Achieving Water Splitting Using Two-Step Photoexcitation Mechanisms. As mentioned above, two-step water-splitting (Z-scheme) systems have significant advantages over conventional one-step systems and they appear to be the most promising way of achieving efficient water splitting under visible light. Bard first proposed a two-step water-splitting system in 1979.[161] Since then, much effort has been expended to construct such a Z-scheme system by focusing on developing new semiconductor materials and effective shuttle redox mediators.[81,162–171] Many researchers have investigated half reactions (i.e., either H_2 or O_2 evolution) by combining various redox mediators with conventional photocatalysts such as TiO_2. Some combinations resulted in gas evolution (either H_2 or O_2) under light irradiation; however, in most cases, gas evolution terminated during the reaction. In photocatalytic reactions with reversible redox mediators, backward reactions readily proceed over the photocatalyst and suppress gas (H_2 or O_2) evolution (Figure 5). Over the H_2 evolution photocatalyst, reduction of Ox to Red (indicated by the broken lines in Figure 5), a thermodynamically advantageous backward reaction, proceeds preferentially over reduction of water to H_2. In contrast, over the O_2 evolution photocatalyst, oxidation of Red to Ox proceeds preferentially over oxidation of water to O_2. Furthermore, it is much more difficult to achieve simultaneous evolution of H_2 and O_2 in two-step water-splitting systems in which the two different photocatalysts coexist in an aqueous solution containing both Red and Ox, because the two reactions have different favorable redox concentrations. For example, a high concentration of Red is favorable for the H_2 evolution photocatalyst, but it causes a significant backward reaction (i.e., reoxidation of Red to Ox) over O_2 evolution photocatalysts, which suppresses O_2 evolution. On the other hand, a high concentration of Ox, which is desirable for the O_2 evolution photocatalyst, reduces the H_2 evolution rate. To realize a two-step water-splitting system, it is thus necessary to develop a photocatalytic system that has a high selectivity for the forward reactions (indicated by the solid lines in Figure 5). Indeed, there had been no report of simultaneous and stoichiometric evolution of H_2 and O_2 even under UV irradiation, prior to our demonstration using a combination of Pt-loaded anatase TiO_2 and bare rutile TiO_2 photocatalysts in the presence of an iodate/iodide (IO_3^-/I^-) shuttle redox mediator,[148] which will be reviewed in Section **2**.

2. Construction of a Two-Step Photoexcitation (Z-Scheme) Water-Splitting System That Uses Two Different TiO_2 Photocatalysts (Anatase and Rutile) in the Presence of an IO_3^-/I^- Shuttle Redox Mediator[77,148,172]

We demonstrated water splitting under visible light for the first time in 2001 using a Z-scheme photocatalytic system that consists of $SrTiO_3$ doped with Cr and Ta (denoted as $SrTiO_3$:Cr/Ta) for H_2 evolution, WO_3 for O_2 evolution, and an iodate/iodide (IO_3^-/I^-) redox couple as an electron mediator (Figure 6),[75–77] which will be introduced in the later Section **3**. Prior to that, Z-scheme photocatalytic water splitting had been demonstrated using a combination of Pt-loaded anatase TiO_2 and bare rutile TiO_2 photocatalysts in the presence of an iodate/iodide (IO_3^-/I^-) shuttle redox mediator.[148] Although this system operates only under UV light ($\lambda < 400$ nm) due to the large band gap of the TiO_2 photocatalysts, it opened the way to achieve water splitting under visible light. The key was controlling the reactivity of electrons and holes with a redox mediator (IO_3^- and I^- anions) and water molecules. This section will review the first demonstrations of water splitting with two-step photoexcitation (Z-scheme) under UV light irradiation using combinations of two different TiO_2 photocatalyst (anatase and rutile).

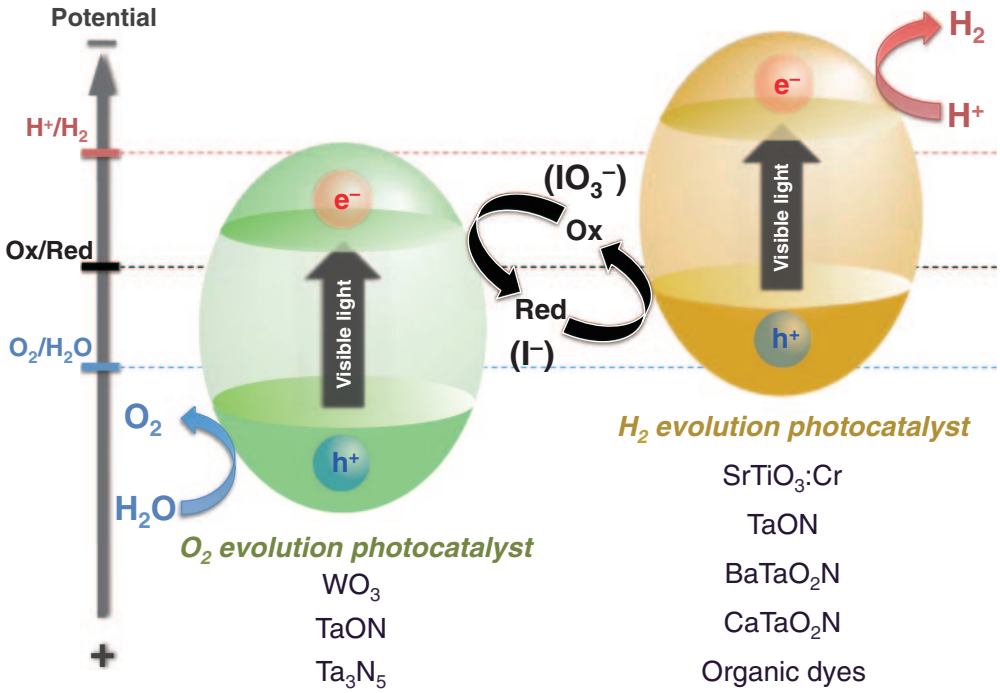

Figure 6. Overview of water splitting of a Z-scheme photocatalysis with an iodate (IO_3^-) and iodide (I^-) ion redox couple.

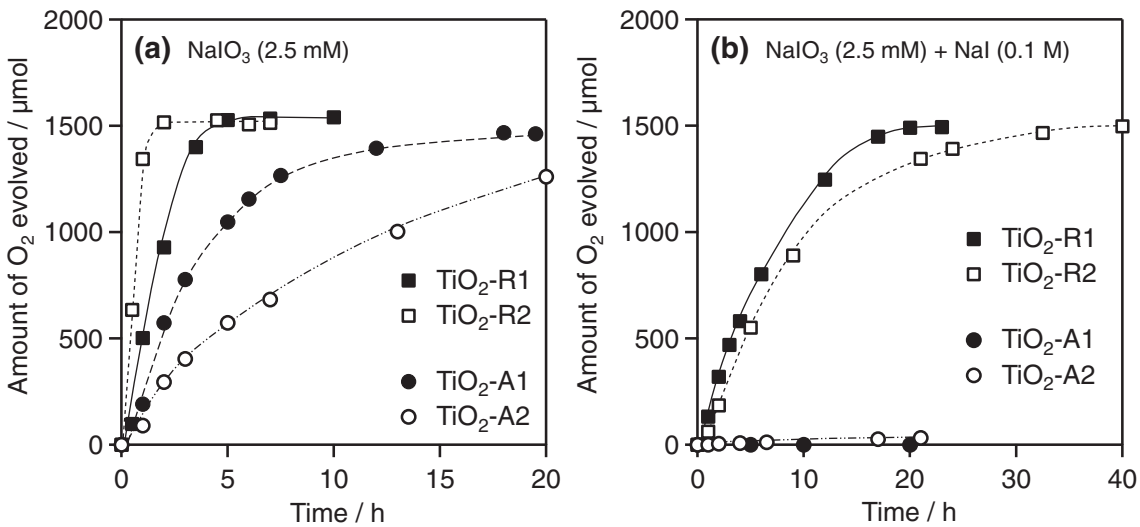

Figure 7. Time course of photocatalytic O_2 evolution over TiO_2 photocatalysts suspended in aqueous solution (400 mL, pH 11 adjusted by NaOH) containing (a) 1 mmol of $NaIO_3$ and (b) 1 mmol of $NaIO_3$ and 40 mmol of NaI.

2.1 Selective Water Oxidation over Rutile TiO_2 Photocatalysts Using IO_3^- as Electron Acceptor under UV Light Irradiation. As mentioned in Section **1–4**, it is quite difficult to achieve simultaneous evolution of H_2 and O_2 in two-step water-splitting systems (Z-scheme) because the backward reactions of the redox mediator proceed readily over both photocatalysts and suppress the forward reactions (H_2 and O_2 evolutions) (Figure 5). Photocatalytic H_2 or O_2 evolutions were investigated using various semiconductor particles suspended in an aqueous solution containing an electron donor (Red) or an electron acceptor (Ox), respectively. Although some combinations of a photocatalyst and a redox mediator resulted in evolution of either H_2 or O_2 under UV or visible light irradiation, gas evolution readily terminated during the reaction due to the backward reaction in most cases. However, efficient and selective O_2 evolution was found to proceed over rutile TiO_2 photocatalysts in an aqueous solution containing IO_3^- anions as electron acceptors (Ox) according to the following reactions:

$$h\nu \rightarrow e^-_{CB} + h^+_{VB} \quad (2)$$

$$IO_3^- + 3H_2O + 6e^-_{CB} \rightarrow I^- + 6OH^- \quad (3)$$

$$2H_2O + 4h^+_{VB} \rightarrow O_2 + 4H^+ \quad (4)$$

Figure 7 shows time courses of O_2 evolution over four TiO_2 photocatalysts (A: anatase; R: rutile) in an aqueous solution (400 mL) containing 1 mmol (2.5 mM) $NaIO_3$ under UV

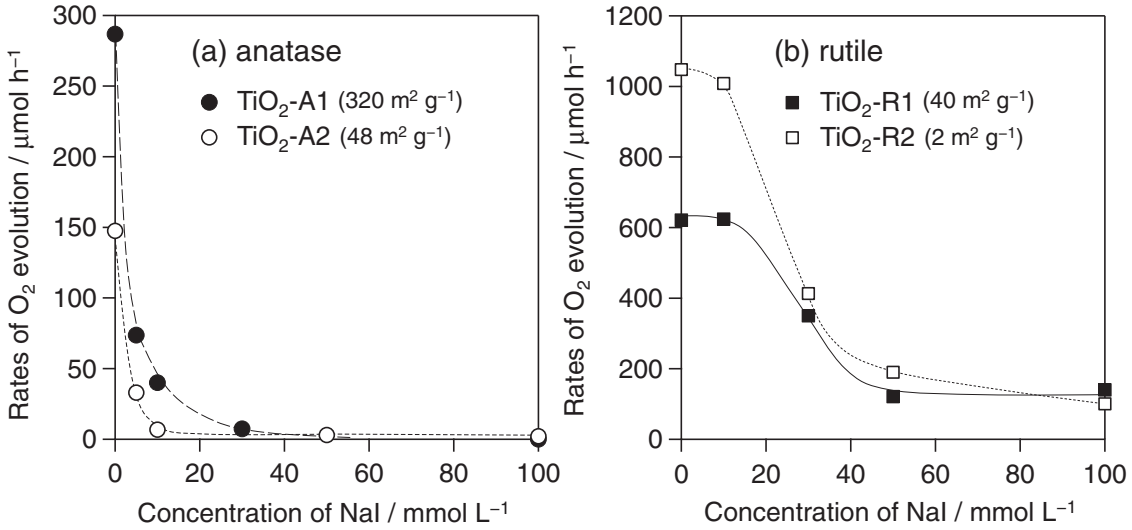

Figure 8. Rates of O_2 evolution over the TiO_2 photocatalysts in the solution containing different concentration of I^- (0–100 mM) and a fixed concentration of IO_3^- (2.5 mM).

irradiation ($\lambda > 300$ nm, 400 W high-pressure Hg lamp). When the reaction was initiated in the absence of I^- anions, O_2 evolution proceeded over both rutile TiO_2 (R1 and R2) and anatase TiO_2 (A1 and A2), while the rutile samples showed higher rates of O_2 evolution than anatase ones. Over the TiO_2-R2 sample, O_2 evolution proceeded with a fairly high efficiency (rate of O_2 evolution: ca. 1 mmol h^{-1}, quantum efficiency at 350 nm: ca. 10%). O_2 evolution over rutile TiO_2 proceeded at an almost constant rate and continued until the total amount of O_2 reached 1.5 mmol in the absence of NaI (Figure 7a) and even in the presence of a considerable amount of I^- (100 mM) in the solution (Figure 7b). The amounts of O_2 (1.5 mmol) agree with the stoichiometric amount (obtained from eqs 3 and 4) expected from the amounts of IO_3^- (1 mmol) added to the solution before irradiation. These behaviors of rutile TiO_2 photocatalysts are quite unique from a thermodynamic viewpoint. The oxidation of water, which is thermodynamically less favorable than the oxidation of I^-, proceeded preferentially over these photocatalysts even in the presence of I^-. On the other hand, such preferential oxidation of water did not take place on anatase TiO_2. As shown in Figure 7a, the rate of O_2 evolution over anatase TiO_2 samples gradually decreased with irradiation time, and the O_2 evolution terminated before it reached the expected stoichiometric value. The different reactivity between anatase and rutile was observed more clearly when the reaction was initiated in the presence of an excess amount of I^-. The addition of excess amount of I^- (100 mM) to the solution completely suppressed O_2 evolution over both the anatase TiO_2 samples, as shown in Figure 7b. Figure 8 shows the rates of O_2 evolution over the TiO_2 photocatalysts in the solution containing different concentration of I^- (0–100 mM) and a fixed concentration of IO_3^- (2.5 mM). The rate of O_2 evolution over anatase TiO_2 photocatalysts markedly decreased with the increasing concentration of I^- (Figure 8a). The O_2 evolution was negligible when the concentration of I^- was above 30 (TiO_2-A1) or 10 mM (TiO_2-A2). It is thus presumed that over anatase TiO_2 photocatalysts, the oxidation of I^-, which is a thermodynamically favorable reaction, proceeds preferentially in the aqueous solution containing a considerable amount of I^-.

$$I^- + 6OH^- + 6h^+_{VB} \rightarrow IO_3^- + 3H_2O \text{ (oxidation of } I^- \text{ to } IO_3^- \text{ by holes)} \quad (5)$$

Consequently, the undesirable recycled reaction ($IO_3^- \rightleftarrows I^-$), the combination of eqs 3 and 5, which consumes electrons (e^-) and holes (h^+), proceeded over the anatase TiO_2 photocatalysts, in place of O_2 evolution. Although the rate of O_2 evolution over rutile TiO_2 also decreased with increasing NaI concentration, appreciable O_2 evolutions were still observed even with considerably high concentration of NaI (above 50 mM), as seen in Figure 8b. This reactivity in oxidation on rutile TiO_2 is quite unique from the thermodynamic standpoint as discussed above. It should be noted that the TiO_2-A2 (surface area: 48 $m^2 g^{-1}$) and the TiO_2-R1 (surface area: 40 $m^2 g^{-1}$), which have similar surface areas, showed quite different reactivity. Thus, the factor governing the reactivity undoubtedly rests on the difference in the crystal structure instead of the surface area.

We also investigated photocatalytic O_2 evolution using I_3^- anion as an electron acceptor instead of IO_3^- anion.

$$I_3^- + 2e^-_{CB} \rightarrow 3I^- \text{ (reduction of } I_3^- \text{ to } I^- \text{ by electrons)} \quad (6)$$

Although appreciable O_2 evolutions were confirmed on some TiO_2 samples, the rates of O_2 evolution were much lower than those in the presence of IO_3^-. These results indicate that the IO_3^- anions can react with electrons more efficiently than I_3^-, despite the similar standard redox potential of the I_3^-/I^- (+0.54 V vs. NHE at pH 7) to that of IO_3^-/I^- (+0.67 V vs. NHE at pH 7).

2.2 Different Reactivity in Oxidation between Anatase and Rutile TiO_2 Photocatalysts. To examine the different reactivity in oxidation of these TiO_2 photocatalysts separately from that in reduction, photoelectrochemical measurements were conducted using two porous TiO_2 photoelectrodes made of the TiO_2-A2 and the TiO_2-R1 powders. The measurements

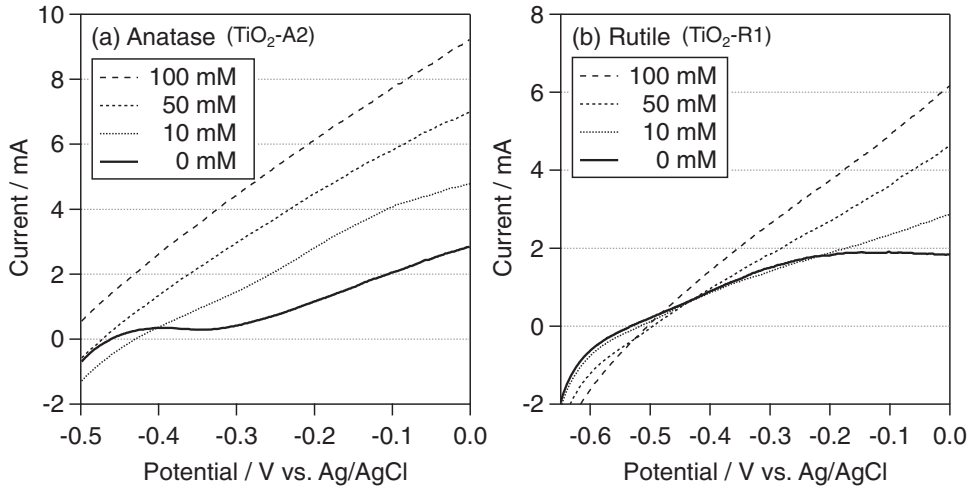

Figure 9. *I–V* characteristics of porous TiO_2 electrodes (ca. 4 cm^2) in an aqueous solution containing different concentrations of NaI from 0 to 100 mM (pH 11, adjusted by NaOH).

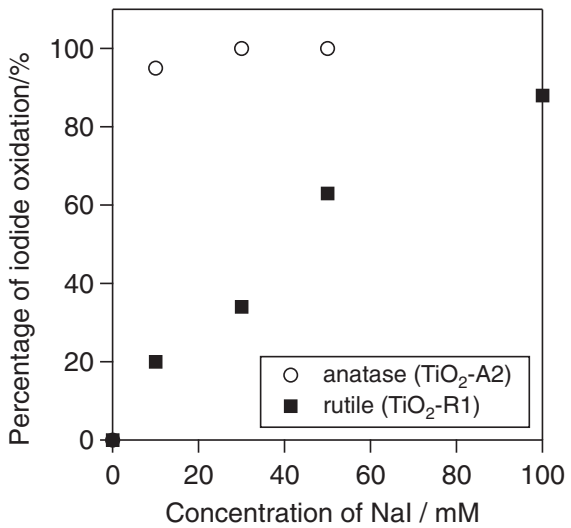

Figure 10. Percentage of oxidation of I^- to the total oxidation current on TiO_2 electrodes in a solution containing different concentrations of NaI (pH 11, adjusted by NaOH).

were carried out using a two-component cell (filled with 10 mM of Na_2SO_4aq., pH 11 adjusted by NaOH) in which a Pt counter electrode was separated from the TiO_2 electrode and a reference electrode (Ag/AgCl) by an ion-exchange membrane (Nafion). The different amounts of NaI were added only into the Na_2SO_4 aqueous solution in which the TiO_2 working electrode and the reference electrode were immersed. The photocurrent over TiO_2-A2 was remarkably increased by the increasing NaI concentration, as shown in Figure 9a. Almost 100% of photogenerated hole over the TiO_2-A2 electrode was consumed for the oxidation of I^- to IO_3^- even with low concentration of I^- (10 mM), as shown in Figure 10. These results indicated that the oxidation of I^- mainly occurred over the TiO_2-A2 powder photocatalyst in the aqueous solution containing I^- above 10 mM. This well agrees with the negligible O_2 evolution over TiO_2-A2 photocatalyst in the presence of more than 10 mM I^-, as shown in Figure 8a. Clearly, the I^- anions act as an effective hole scavenger on the anatase TiO_2. On the other hand, the increase of photocurrent over the TiO_2-R1 electrode was negligibly small by adding 10 mM of I^-, as shown in Figure 9b. Approximately 80% of the photogenerated holes were still consumed to oxidize H_2O to O_2, while the remainder was consumed to oxidize I^- to IO_3^- (Figure 10). Although both the photocurrent and the percentage of I^- oxidation increased with the increasing I^- concentration, the oxidation of water still proceeded over the TiO-R1 electrode even in the presence of 50 mM of I^-. This also agreed with the results of the O_2 evolution over TiO_2-R1, as shown in Figure 8b. These results clearly indicate that anatase and rutile have a different reactivity in the competitive oxidation of I^- and H_2O. Ohno and co-workers have also reported the preferential oxidation of H_2O over rutile TiO_2 photocatalysts in the presence of an Fe^{3+}/Fe^{2+} redox couple.[167] Therefore, rutile itself surely possesses an active site for the effective oxidation of H_2O, as suggested by some research. For example, Nakato and co-workers have suggested that the (100) face of rutile TiO_2 possesses favorable properties for water oxidation.[173] Ohno and co-workers studied the role of the crystal faces of anatase and rutile TiO_2 particles in photocatalytic reactions.[174] It was suggested that the well-developed crystal faces help in the separation of electrons and holes in the TiO_2 particle. This effect was found to be much stronger for the rutile particles than for the anatase particles.[174] The efficient charge separation in rutile particles may increase the concentration of holes on the particular crystal faces such as (100) and consequently facilitate the water oxidation.

2.3 Adsorption Properties of IO_3^- and I^- on TiO_2 Powders in Aqueous Solution. The different adsorption properties of IO_3^- and I^- anions by these TiO_2 photocatalysts also explain their different reactivities when IO_3^- and I^- coexist. The amounts of IO_3^- and I^- ions adsorbed on TiO_2 particles were determined by analyzing the concentration of the anions in the aqueous solution before and after the addition of measured amounts of photocatalyst powder (1–2 g) to the solution (1 mL) in darkness. After leaving the solution in

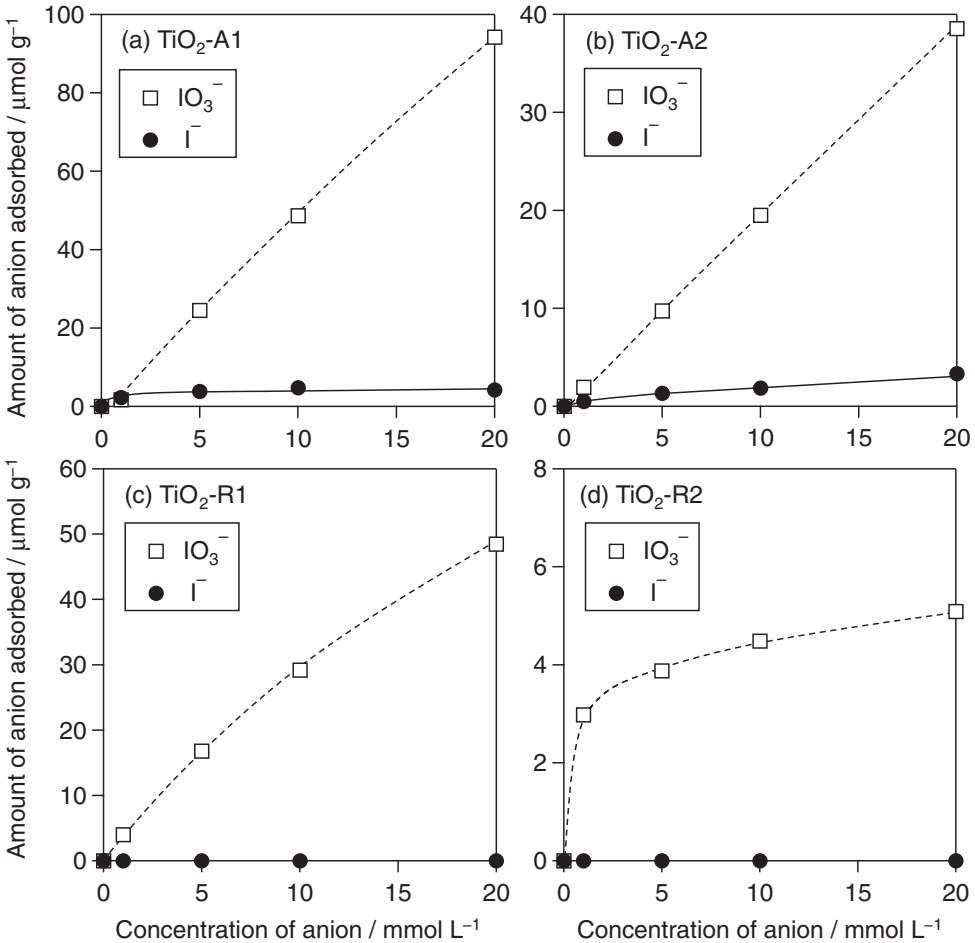

Figure 11. Adsorption properties of iodate (IO_3^-) and iodide (I^-) anions on various TiO_2 powders.

darkness at room temperature for 12 h, the concentrations of anions remaining in solution were measured by ion chromatography. Interestingly, IO_3^- ions readily adsorb on the surface of rutile TiO_2 particles (Figures 11c and 11d), whereas I^- ions adsorb very little on them (below the detection limit). The different adsorption properties of IO_3^- and I^- anions by these photocatalysts explain the unusual reactivity of rutile TiO_2 photocatalysts, the efficient and preferential water oxidation in the coexistence of IO_3^- and I^- anions. That is, even in the low concentrations, IO_3^- anions readily adsorb onto the surface of rutile TiO_2 particles and efficiently react with photoexcited electrons there. Meanwhile, photogenerated holes can preferentially react with water molecules to produce O_2 because the I^- oxidation rate, which competes with water oxidation, is low due to the negligible adsorptivity of I^- ions on the surface of rutile TiO_2 (Figure 12a). In contrast, both IO_3^- and I^- ions adsorbed on the surface of anatase TiO_2 (Figures 11a and 11b), while IO_3^- showed a higher adsorptivity than I^- at higher concentrations. The appreciable adsorption of I^- anions on anatase TiO_2 particles is undoubtedly responsible for the efficient oxidation of I^- to IO_3^- (or I_3^-), which is thermodynamically more favorable than water oxidation, by photogenerated holes on these photocatalysts and for completely suppressing oxidation of water to O_2 (Figure 12b).

From these results, we can conclude that the rutile TiO_2 photocatalysts have a unique property of oxidation, which enables preferential oxidation of H_2O to O_2 in the presence of IO_3^- and I^- anions, regardless of the thermodynamic disadvantage of water oxidation when compared to the oxidation of I^-. The distinct difference between the adsorption properties of the IO_3^- and I^- anions on rutile TiO_2 particles is undoubtedly one of the major factors enabling selective and efficient water oxidation, while the origin of the different adsorption properties between anatase and rutile is not clarified yet. This high selectivity for the forward reaction (O_2 evolution) is exactly what we have desired to find, and is indispensable to achieve overall water splitting, i.e., simultaneous evolution of H_2 and O_2, through the two-step photoexcitation between two different photocatalysts, which will be demonstrated in a later Section **2.5**.

2.4 Photocatalytic H_2 Evolution over Pt-Loaded TiO_2 Photocatalysts Using I^- as an Electron Donor. The above results (Figures 8–10) indicated that I^- anions act as an efficient electron donor over anatase TiO_2 photocatalysts. Indeed, the Pt-loaded anatase TiO_2 photocatalysts showed reasonable activity for H_2 evolution in the presence of I^- under UV light irradiation. As summarized in Table 1, Pt–anatase TiO_2 exhibited higher activity for H_2 production than Pt–rutile TiO_2. Figure 13 shows the time courses of the H_2 evolution over Pt(0.5 wt %)–TiO_2-A1 suspended in a NaI (0.1 M) aqueous solution with different pH values. In an acidic aqueous solution of pH <5, the triiodide (I_3^-) anion was mainly

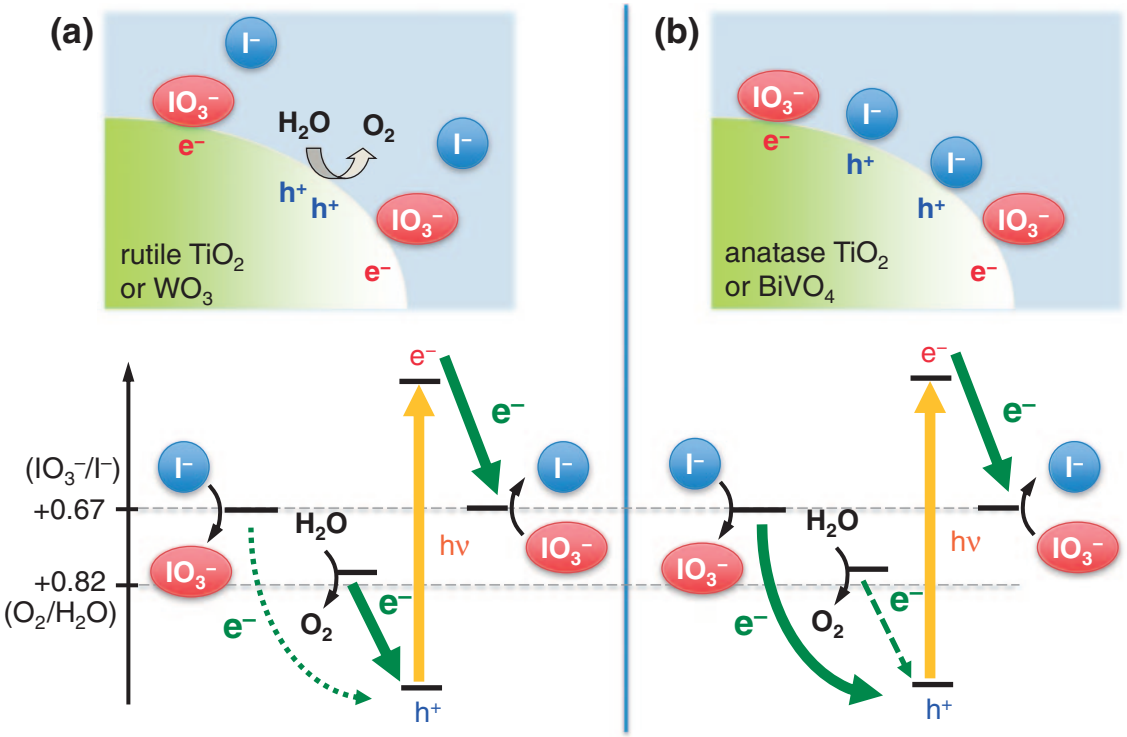

Figure 12. Schematic illustration of photocatalytic reactions with iodate (IO_3^-) and iodide (I^-) anions.

Table 1. Photocatalytic Activity of Various Photocatalysts Suspended in Aqueous NaI Solution[a)]

Photocatalyst[b)]	Surface area /$m^2\,g^{-1}$	Rate of gas evolution[c)] /$\mu mol\,h^{-1}$	
		H_2	O_2
1 Pt–TiO_2-A1	320	20[d)]	tr.
2 Pt–TiO_2-A2	48	6[d)]	tr.
3 TiO_2-A1	320	0	0
4 TiO_2-A2	48	0	0
5 Pt–TiO_2-R1	40	tr.	0
6 Pt–TiO_2-R2	2	tr.	0
7 TiO_2-R1	40	0	0
8 TiO_2-R2	2	0	0
9 Pt–TiO_2-A1 + TiO_2-R1		125	62
10 Pt–TiO_2-A1 + TiO_2-R2		180	90
11 Pt–TiO_2-A2 + TiO_2-R1		8	4
12 Pt–TiO_2-A2 + TiO_2-R2		18	9
13 Pt–TiO_2-R1 + TiO_2-A1		<1	tr.
14 Pt–TiO_2-A1 + TiO_2-A2		tr.	tr.
15 Pt–TiO_2-A1 + Pt–WO_3		95	47
16 Pt–TiO_2-A1 + Pt–$BiVO_4$		tr.	0

a) Catalyst: 0.5 g (in the case of mixture 0.25 + 0.25 g, 0.5 wt % of Pt cocatalyst was loaded), water 400 mL, NaI 40 mmol (pH 11 for Entries 1–14, pH 6.5 for Entries 15 and 16), Pyrex reactor of inner irradiation type, high-pressure Hg lamp (400 W). b) TiO_2-A1 (anatase, Ishihara ST-01); TiO_2-A2 (anatase, prepared by hydrolysis of titanium tetrapropoxide); TiO_2-R1 (rutile, Ishihara TTO-55N); TiO_2-R2 (rutile, Toho Titanium HT0201). c) Rate in steady state. d) Initial rate.

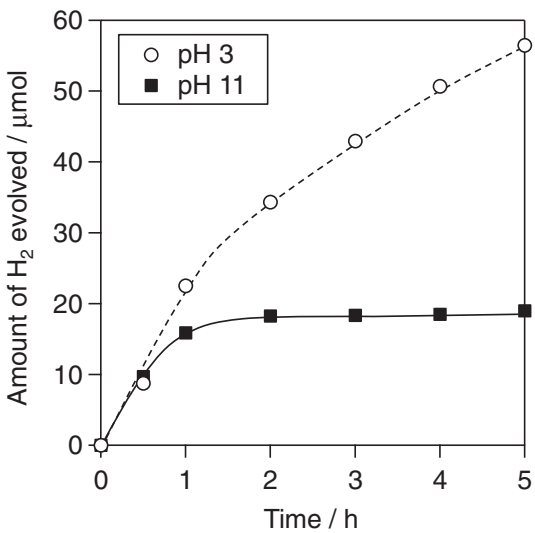

Figure 13. Time course of photocatalytic evolution of H_2 using Pt(0.5 wt %)–TiO_2-A1 (anatase, Ishihara ST-01) photocatalyst suspended in 0.1 M of NaI aqueous solution under UV light irradiation ($\lambda > 300$ nm, 400 W Hg lamp).

produced as the oxidative product of I^- with H_2 evolution, as reported by Ohno and co-workers.[165] We found the IO_3^- anion produced over the Pt–anatase TiO_2 photocatalysts as the oxidative product of I^- in a basic solution of pH >9. In solutions of pH 5 to 9, both I_3^- and IO_3^- were produced. These results indicate that the following reactions had taken place over a Pt–anatase TiO_2 photocatalyst under UV light irradiation, along with the oxidation of I^- to IO_3^- (eq 5):

$$2H^+ + 2e^-_{CB} \rightarrow H_2 \text{ (reduction of water to } H_2 \text{ by electrons)} \quad (7)$$

$$3I^- + 2h^+_{VB} \rightarrow I_3^- \text{ (oxidation of } I^- \text{ to } I_3^- \text{ by holes)} \quad (8)$$

The IO_3^- anions in neutral and basic solutions were possibly produced via the disproportional reaction from I_3^-:

$$3I_3^- + 6OH^- \rightarrow 8I^- + IO_3^- + 3H_2O \quad (9)$$

The rates of H_2 evolution gradually decreased with the irradiation time, as seen in Figure 13. The H_2 evolution terminated when the concentration of the product (I_3^- or IO_3^-) in the solution reached a certain level. These results indicate that the backward reactions, the reduction of I_3^- (eq 6) or IO_3^- (eq 3), proceeded on the reduction sites of the photocatalyst. The facile termination of H_2 evolution in the basic solution proves that the IO_3^- anions react more efficiently than I_3^-, as described in a previous Section **2.1**.

2.5 Simultaneous Evolution of H_2 and O_2 Using a Mixture of Pt–TiO_2-Anatase and TiO_2-Rutile under UV Light Irradiation. We thus attempted water splitting using a combination of Pt–anatase TiO_2 for H_2 evolution and rutile TiO_2 for O_2 evolution, respectively. Figure 14 shows the time course of gas evolution using the mixture of Pt(0.5 wt %)–TiO_2-A1 and bare TiO_2-R2 suspended in a basic aqueous solution of NaI (0.1 M, pH 11), in which simultaneous evolution of H_2 and O_2 in a stoichiometric ratio was observed. The rate of gas evolution gradually decreased with gas accumulation in the closed system, possibly because the backward reaction from the evolved H_2 and O_2 into H_2O also proceeded on Pt metal cocatalyst particles.[8,9,175] However, the initial rate of gas evolution was recovered by the evacuation of accumulated gases. When a 200 h long-term photoirradiation was carried out in an aqueous solution of NaI (40 mM, pH 11) with periodical evacuation of gas phase, the total amount of H_2 and O_2 reached ca. 15.6 and 7.8 mmol, respectively. The amount of H_2 gas evolved exceeded the stoichiometric amount of TiO_2 powders (6.3 mmol) and I^- (14 mmol) in the solution. The stoichiometric evolution of H_2 and O_2 was also observed in an aqueous solution of LiI and KI, but not in that of NaBr, NaCl, or NaOH. As Table 1 shows, only the combination of Pt–anatase TiO_2/rutile TiO_2 exhibited simultaneous evolution of H_2 and O_2 in a stoichiometric ratio (Runs 9–12). Simultaneous evolution of H_2 and O_2 was not observed when these photocatalysts were used alone (Runs 1–8) or in other combinations such as Pt–rutile TiO_2/anatase TiO_2 (Run 13) or Pt–anatase TiO_2/anatase TiO_2 (Run 14). These results demonstrate that overall water splitting proceeds by a two-step photoexcitation mechanism combined with a redox cycle between anions IO_3^- and I^-. The first step involves reduction of water to H_2 and oxidation of I^- to IO_3^- over a Pt–anatase TiO_2 photocatalyst, while the second step involves reduction of IO_3^- to I^- and oxidation of water to O_2 over a rutile TiO_2 photocatalyst. The initial H_2 evolution rates over the combined Pt–anatase TiO_2/rutile TiO_2 systems (Runs 9–12) are much higher than over Pt–anatase TiO_2 alone (Runs 1–4) (Figures 13, 14 and Table 1). The rapid reduction of IO_3^- to I^- over rutile TiO_2 can maintain a very low IO_3^- concentration during the reaction, effectively suppressing the undesirable backward reaction (IO_3^- reduction to I^-) over the Pt–anatase TiO_2 photocatalyst, and thus giving a higher H_2 evolution rate. The key for achieving water splitting is to use different oxidation reactions; in other words, preferential oxidation of I^- to IO_3^- over the H_2 photocatalyst (e.g., Pt–anatase TiO_2) and preferential oxidation of water to O_2 over the O_2 photocatalyst (e.g., rutile TiO_2) must occur simultaneously in a single solution.

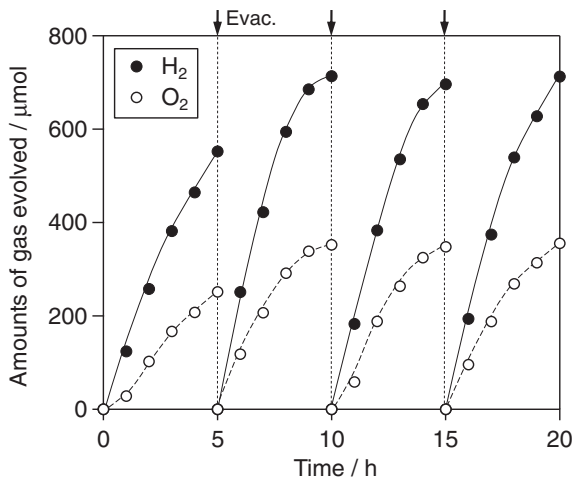

Figure 14. Time courses of photocatalytic evolution of H_2 and O_2 using a mixture of Pt–TiO_2-A1 and TiO_2-R2 photocatalysts from 0.1 M aqueous NaI solution (pH 11, adjusted by NaOH) under UV light.

The apparent quantum efficiency of the overall water splitting was ca. 4% at 350 nm using the combination of Pt(0.5 wt %)–TiO_2-A1 and TiO_2-R2 in a basic aqueous solution of NaI (0.1 M, pH 11). When the Pt(0.5 wt %)–TiO_2-A1 was independently used in the same solution, the apparent quantum efficiency for the initial rate of H_2 evolution was determined to be ca. 1%. On the other hand, ca. 10% of high quantum efficiency was obtained in O_2 evolution over TiO_2-R2 in a 2.5 mM of $NaIO_3$ aqueous solution (pH 11), and ca. 4% in the aqueous solution containing both $NaIO_3$ (2.5 mM) and NaI (0.1 M). These results indicate that the rate-determining step in the combination system is the H_2 and IO_3^- productions over Pt–TiO_2-A1 photocatalyst. Therefore the overall efficiency will be improved by applying H_2 evolution photocatalyst with higher activity.

2.6 Effect of pH and NaI Concentration on Water Splitting Using a Combination of Pt–TiO_2-Anatase and TiO_2-Rutile. Figure 15a shows the rates of gas evolution over the mixture of Pt(0.5 wt %)–TiO_2-A1 and bare TiO_2-R2 suspended in 0.1 M of NaI aqueous solutions with different pH values. The rates significantly increased with increasing pH from 3 to 9 and then decreased above 11. The O_2 evolution was negligible at pH 3 because the main oxidative product over Pt–anatase TiO_2 photocatalysts was I_3^-, which cannot work as an efficient electron acceptor for O_2 evolution over rutile TiO_2 photocatalysts, as described in a previous Section **2.1**. At pH 5 to 7, O_2 evolution was observed after some induction period. The amounts of O_2 in these cases, however, were less than the stoichiometric ratio to the H_2 evolved, certainly due to the accumulation of I_3^- in the solution. The induction period suggests that some IO_3^- anions were produced via the disproportional reaction from I_3^- (eq 9) in the aqueous solutions

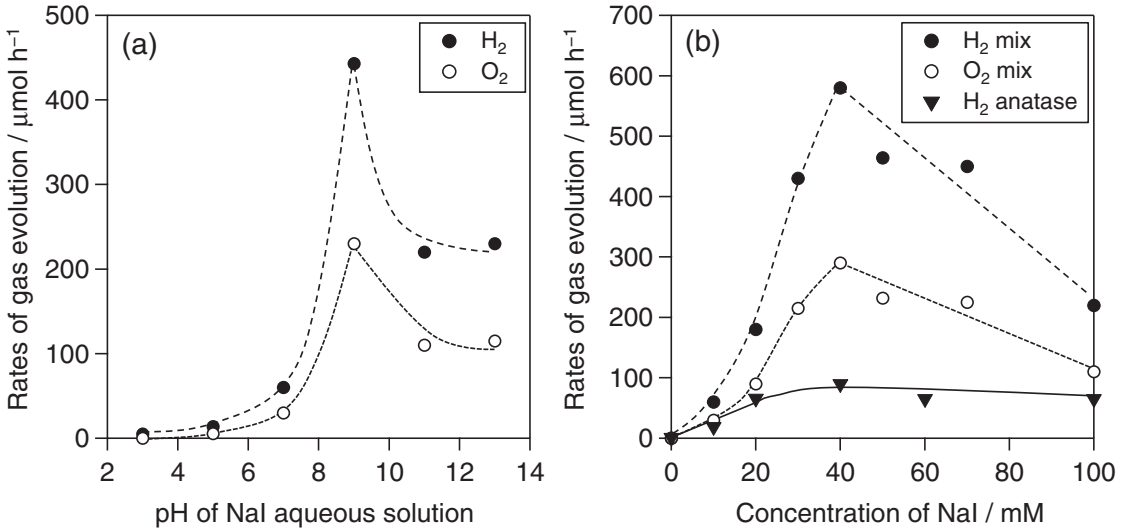

Figure 15. (a) Dependence of rates of gas evolution over a mixture of Pt–TiO_2-A1 and bare TiO_2-R2 photocatalysts upon the pH value of NaI solution (NaI: 0.1 M). (b) Dependence of rates of gas evolution over a mixture of Pt–TiO_2-A1 and bare TiO_2-R2 photocatalysts upon the concentration of NaI aqueous solution (pH 11).

during the photocatalytic reaction. The accumulation of I_3^- also causes a light loss owing to the strong light absorption of I_3^- anion at around 350 nm, resulting in a lowered efficiency of the photocatalysis on TiO_2 particles. In basic solutions of pH $\geq$9, the simultaneous evolution of H_2 and O_2 with a stoichiometric ratio was observed from the initial period of photoirradiation. It can be therefore concluded that basic conditions of above pH 9 result in high efficiencies for overall water splitting under UV light over a combination of Pt–anatase TiO_2 and rutile TiO_2 in the presence of a IO_3^-/I^- shuttle redox mediator, due to the efficient redox cycle between IO_3^- and I^- under basic conditions without forming other unfavorable intermediates such as I_3^-.

As shown in Figure 15b, the rate of water splitting greatly increased with increasing NaI concentration up to 40 mM, and gradually decreased above 40 mM. The presence of I^- anions, even at such low concentrations as 10 mM, resulted in the overall water splitting in a stoichiometric ratio. When the Pt(0.5 wt %)–TiO_2-A1 was used alone, the rate of H_2 evolution increased with increasing concentration of NaI up to 40 mM, and then almost saturated at higher concentrations, as seen in Figure 15b. As suggested by the quantum efficiency, the H_2 evolution over the Pt–anatase TiO_2 photocatalyst appeared to be the rate-determining step in the overall reaction. Therefore, it seems quite reasonable that the rate of overall water splitting increases with the increased rate of H_2 evolution over the Pt–anatase TiO_2. However, the higher concentration of I^- results in the decrease in the rate of O_2 evolution over rutile TiO_2 photocatalyst due to the increased rate of the competitive oxidation of I^-, as indicated by the results in Figures 8 and 10. Thus the efficiency of overall water splitting gradually decreased with the increasing NaI concentration above 40 mM. In the two-step water-splitting system based on the electron transfer between the two different photocatalysts via redox cycle of mediator, the concentration of the redox mediator significantly affects the overall efficiency mainly due to the occurrence of backward reactions on each photocatalysts.

2.7 Suppression of Backward Water Formation by Iodide Coating on Pt Cocatalyst. Most semiconductor photocatalysts that have been developed to date need to be loaded with suitable cocatalyst particles to promote H_2 production. Noble metals such as Pt are effective cocatalysts that enhance water reduction to generate H_2 in the presence of a sacrificial electron donor such as methanol. However, noble metals such as Pt cannot be used as cocatalyst for overall water splitting because they are efficient catalysts for the backward reaction from H_2 and O_2 to H_2O. It was confirmed that Pt-loaded photocatalysts such as Pt–TiO_2 could not split water into H_2 and O_2 in a simple aqueous suspension system, because the H_2 and O_2 produced over the photocatalyst rapidly react back to H_2O on Pt surface before they escape from the suspension to gas phase.[8,9,175] The Z-scheme water-splitting system based on IO_3^-/I^- redox couple, however, can generate H_2 and O_2 simultaneously even in the presence of Pt cocatalyst on the anatase TiO_2 photocatalyst. It was found that the iodide (I^-) anion was adsorbed preferentially onto Pt cocatalyst and spontaneously formed an iodine layer, which effectively suppressed the backward reaction of water formation.[172] Figure 16c shows the I 3d and Pt 4f XPS spectra of 3 wt % Pt-loaded TiO_2-A1 after 20 h of photoreaction in an aqueous solution of NaI (1 mM). Strong peaks were observed at 618.5 and 630 eV. These peaks were also observed over a Pt–TiO_2-A1 photocatalyst stirred in NaI(aq) for 12 h in the dark (Figure 16b), but not over bare TiO_2-A1, as shown in Figure 16d. Soriaga et al. have reported that I^- anions in aqueous solution were spontaneously and oxidatively chemisorbed as zero-valent I atoms on a Pt polycrystalline electrode and formed a stable monolayer on the Pt surface.[176] The binding energies of I $3d_{5/2}$ and I $3d_{3/2}$ observed over the Pt–TiO_2 were in fair agreement with those over the Pt polycrystalline electrode. As shown in Figure 17, the pressure of a gas mixture of H_2 and O_2 rapidly decreased in the case of the fresh Pt–TiO_2 due to the water formation from H_2 and O_2 on naked Pt surface. On the other hand, the pressure of the mixture

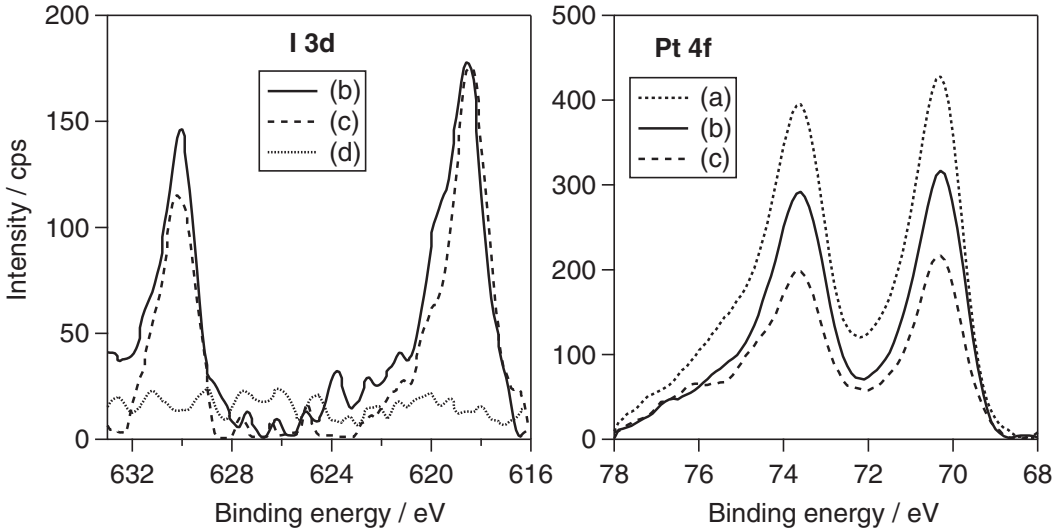

Figure 16. X-ray photoelectron spectra of I 3d and Pt 4f for Pt(3 wt %)–anatase TiO_2 powders; fresh sample (a), after stirring in an aqueous solution of NaI (1 mM) for 12 h in the dark (b), after photoreaction in an aqueous solution of NaI (1 mM) for 20 h under UV light irradiation (c). X-ray photoelectron spectrum of I 3d for bare anatase TiO_2 powder after stirring in an aqueous solution of NaI (1 mM) for 12 h in dark (d).

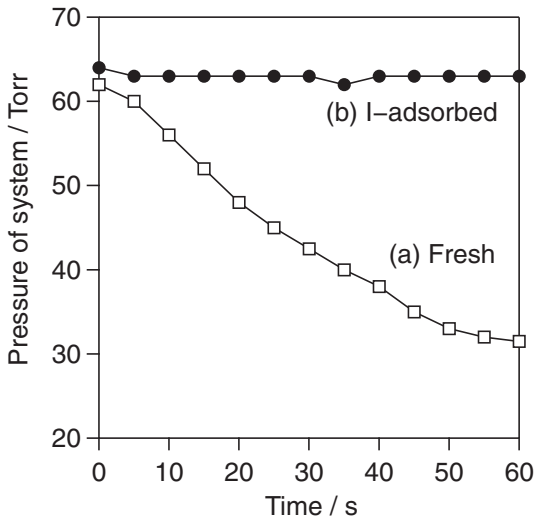

Figure 17. Water formation from H_2 and O_2 in gas phase reaction over (a) fresh and (b) I-adsorbed 3 wt % Pt–TiO_2 photocatalyst powders. A mixture of H_2 and O_2 (H_2:O_2 = 2:1) gases was introduced to a closed gas-circulating system with a Pyrex glass cell containing 10 mg of photocatalyst powder without water.

decreased much more slowly in the case of I-adsorbed Pt–TiO_2 photocatalyst: it took about 2 h until the gas pressure reached 30 Torr. This indicates that the Pt metal surface modified by I^- effectively suppresses the backward reaction from H_2 and O_2. Soriaga et al. reported that electron transfer could occur through the iodine layer formed on the Pt surface, while the conductivity of the I-adsorbed surface was slightly lower than that for bare Pt surface. They also reported that the iodine could be reductively eliminated from the surface either by exposure to electrogenerated H_2 or by application of sufficiently negative potentials.[176] Therefore, the following two mechanisms can be suggested for the H_2 production over I-adsorbed Pt surface: (1) photogenerated electrons migrate from bulk Pt to the surface of the iodine layer and reduce H^+ to H_2; and (2) a part of the iodine layer is reductively eliminated by photogenerated electrons, and the reduction of H^+ to H_2 takes place on the bare Pt surface.

These results strongly suggested that the iodide anions serve not only as an electron mediator between two photocatalyst systems but also as inhibitor of backward water formation reaction on Pt cocatalyst, thus resulting in sustained water splitting under UV light. Kudo et al. also reported that the Fe^{3+}/Fe^{2+} redox couple functioned not only as electron mediator but also as inhibitor of backward reaction on Pt in their Z-scheme water-splitting systems.[151,152]

2.8 Summary. A new photocatalytic system that splits water into H_2 and O_2 was designed using a two-step photoexcitation system composed of an IO_3^-/I^- redox mediator and two different TiO_2 photocatalysts: Pt-loaded anatase for H_2 evolution and rutile for O_2 evolution, respectively. Photocatalytic O_2 evolution proceeded at a steady rate over rutile TiO_2 photocatalysts, continuing until almost all IO_3^- ions in the solution were reduced to I^-. The characteristic property of this reaction is that the oxidation of water to O_2, which is thermodynamically less favorable than the oxidation of I^-, proceeds efficiently even at considerably high I^- concentrations. It was found that IO_3^- anions readily adsorbed onto the surface of rutile TiO_2 particles, while I^- anions barely adsorbed. These results strongly suggested that the photoexcited electrons could react efficiently with the IO_3^- adsorbed on the rutile surface, whereas the photogenerated holes could react with water molecules selectively due to the negligibly low adsorptivity of I^- on rutile. On the other hand, both IO_3^- and I^- anions adsorbed on anatase TiO_2 particles. This could well explain the results observed for Pt-loaded anatase TiO_2, which indicated that H_2 evolution proceeded efficiently on Pt–anatase TiO_2 accompanied by I^- oxidation during the initial period but was significantly inhibited by the accumulation of IO_3^- in the

Table 2. Rates of O_2 Evolution over WO_3 and $BiVO_4$ Photocatalysts Suspended in $NaIO_3$ or $AgNO_3$ Aqueous Solution under Visible Light[a)]

Photocatalyst	Rate of O_2 evolution /μmol h^{-1}
WO_3 (IO_3^- acceptor)[b)]	tr.
Pt(0.5 wt %)–WO_3	75
RuO_2(0.5 wt %)–WO_3	22
IrO_2(0.5 wt %)–WO_3	15
$BiVO_4$	2
Pt(0.5 wt %)–$BiVO_4$	22
RuO_2(0.5 wt %)–$BiVO_4$	10
IrO_2(0.5 wt %)–$BiVO_4$	20
WO_3 (Ag^+ acceptor)[c)]	126
$BiVO_4$	240

a) Catalyst: 0.25 g, water 250 mL, Pyrex reactor of outer irradiation type, Xe lamp (400 W) with a cut-off filter (Hoya, L-42). b) $NaIO_3$: 1 mmol. c) $AgNO_3$: 2.5 mmol.

solution. The combination of two different TiO_2 photocatalysts results in a stoichiometric evolution of H_2 and O_2 via the redox cycle of IO_3^- and I^-. The first step involves reduction of water to H_2 and oxidation of I^- to IO_3^- over a Pt–anatase TiO_2 photocatalyst, while the second step involves reduction of IO_3^- to I^- and oxidation of water to O_2 over a rutile TiO_2 photocatalyst. This reaction mechanism is new and significantly different from conventional water-splitting systems. Although this system operates only under UV light ($\lambda <$ 400 nm) due to the large band gap of the TiO_2 photocatalysts, it has opened a path to achieve water splitting under visible light, which will be reviewed in the next section.

3. First Demonstration of Overall Water Splitting under Visible Light Using a Combination of Two Different Visible-Light-Responsive Oxide Photocatalysts[75–77]

As described above, Z-scheme water splitting under UV light has been achieved for the first time by using Pt-loaded anatase TiO_2 as the H_2 photocatalyst together with rutile TiO_2 for O_2 evolution in the presence of IO_3^-/I^- redox mediator. Based on these findings, we started to seek visible-light-responsive photocatalysts that posses high selectivity toward O_2 evolution even in the presence of IO_3^- and I^-, similar to rutile TiO_2 photocatalysts. We found that the selective oxidation of water also proceeded over a tungsten trioxide (WO_3) loaded with Pt. $SrTiO_3$ codoped with Cr and Ta was then found to be active for both H_2 and IO_3^- production from an aqueous NaI solution under visible light irradiation, after loading of Pt cocatalyst. Using a combination of these photocatalysts resulted in simultaneous H_2 and O_2 evolution in a stoichiometric ratio from NaI aqueous solution under visible light. This was the first demonstration of water splitting into H_2 and O_2 under visible light irradiation. In this section, the first demonstration of visible light driven water splitting will be reviewed.

3.1 Selective Water Oxidation over Pt-Loaded WO_3 Photocatalysts Using IO_3^- as Electron Acceptor under Visible Light Irradiation. As shown in Table 2, WO_3 and $BiVO_4$ photocatalysts were found to show activity for water

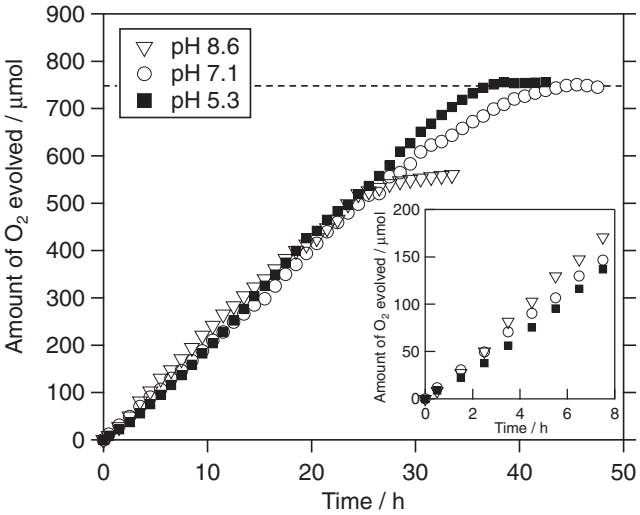

Figure 18. Photocatalytic O_2 evolution over the Pt(0.5 wt %-Imp-823)–WO_3 photocatalyst (0.3 g) using iodate (IO_3^-) as an electron acceptor at different pH values under visible light. The reaction was carried out in an aqueous solution (250 mL) containing both $NaIO_3$ (2 mM) and NaI (5 mM). The broken line shows the upper limit of O_2 evolution (750 μmol) expected from the amount of IO_3^- (500 μmol) added to the solution.

oxidation to O_2 in the presence of the IO_3^- electron acceptor under visible light irradiation ($\lambda > 410$ nm), while the loading of cocatalyst such as Pt was indispensable for the efficient O_2 evolution. Figure 18 shows the time course of O_2 evolution over the Pt-loaded WO_3 sample, which was prepared by impregnation with calcination at 823 K in air, in an aqueous solution (250 mL) containing both $NaIO_3$ (2 mM) and NaI (5 mM) at different pH values. Under weakly acidic (pH 5.3) and neutral (pH 7.1) conditions, O_2 evolution proceeded at an almost steady rate and continued until the total amount of O_2 reached 750 μmol, which is the expected value from the amount of IO_3^- (500 μmol). Although the rate of O_2 evolution over Pt–WO_3 photocatalyst was lowered by the increasing concentration of NaI added into the solution (Figure 19a), the O_2 evolution was found to proceed at a steady rate until it reached the expected value, similar to the case of rutile TiO_2 photocatalyst. On the other hand, the addition of excess I^- into the solution completely suppressed O_2 evolution over Pt–$BiVO_4$ photocatalyst, as shown in Figure 19a. This strongly suggested that the undesirable backward reaction, oxidation of I^- to IO_3^- (or I_3^-), preferentially proceeded over the Pt–$BiVO_4$ photocatalyst instead of the oxidation of H_2O to O_2. The same trend was observed in reactions under UV light irradiation, as shown in Figure 19b.

The different reactivity between WO_3 and $BiVO_4$ can be explained by the distinctly different adsorption between IO_3^- and I^- anions on the surface of these photocatalyst powders, analogous to the case of TiO_2 (Section **2.3**). As seen in Figure 20a, IO_3^- anions are readily adsorbed on the surface of WO_3 particles, whereas I^- anions show no adsorptivity in the range of NaI concentration up to 20 mM. Therefore, it appears that IO_3^- anions, even in quite low concentrations, can adsorb on the surface of WO_3 and react with the photoexcited electrons

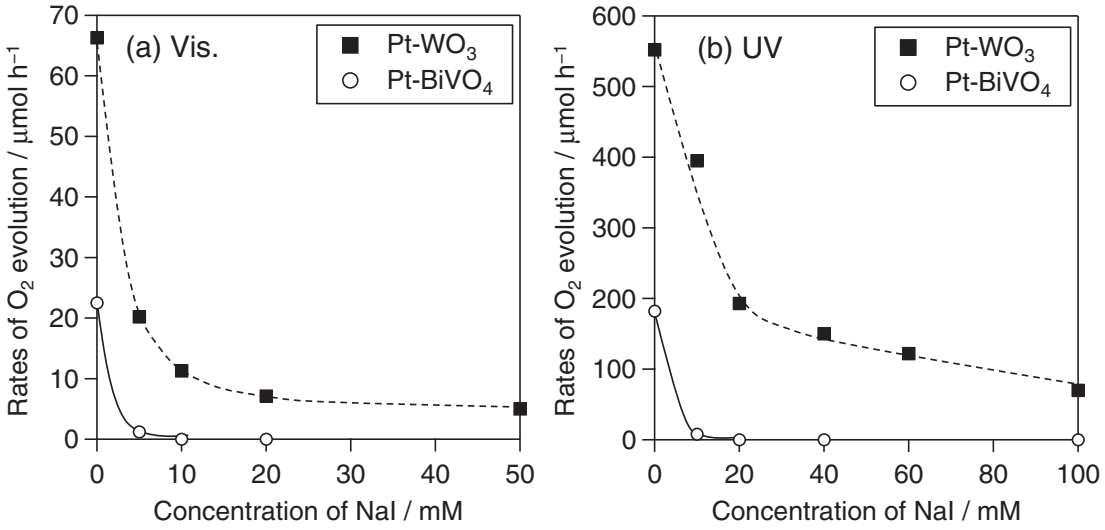

Figure 19. Rates of O_2 evolution over the Pt(0.5 wt %)-loaded WO_3 and $BiVO_4$ photocatalysts suspended in the solution containing different concentration of I^- (0–100 mM) and a fixed concentration of IO_3^- (2.5 mM). (a) Under visible light irradiation ($\lambda > 410$ nm, emitted by 300 W Xe lamp); (b) under UV light irradiation ($\lambda > 300$ nm, emitted by 400 W high pressure Hg lamp).

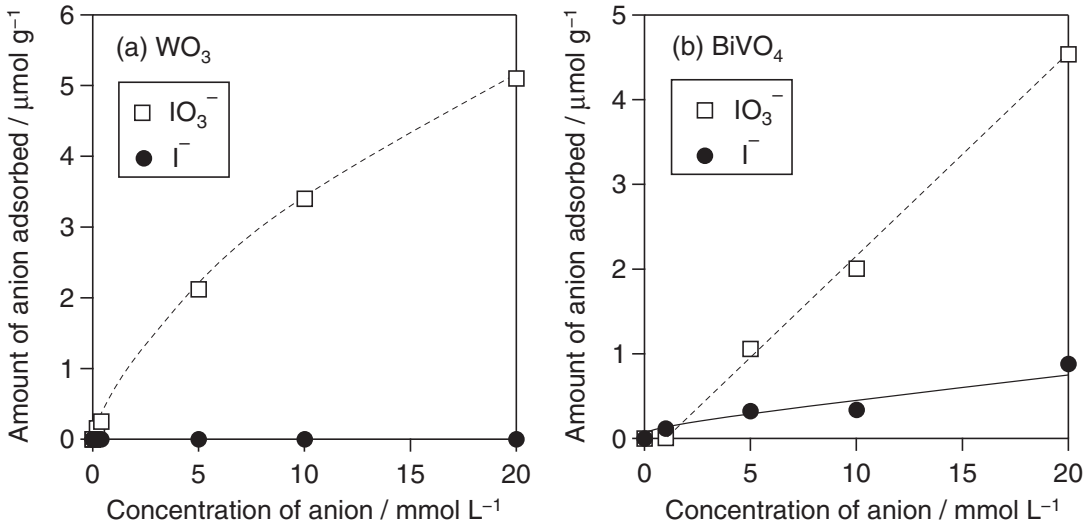

Figure 20. Adsorption properties of iodate (IO_3^-) and iodide (I^-) anions on (a) WO_3 and (b) $BiVO_4$ powders.

efficiently. Meanwhile, photogenerated holes can preferentially react with water molecules to produce O_2 because the I^- oxidation rate, which competes with water oxidation, is low due to the negligible adsorptivity of I^- ions on the surface of WO_3 (Figure 12a). On the other hand, both IO_3^- and I^- adsorbed on the surface of $BiVO_4$, as shown in Figure 20b, similar to the behavior in anatase TiO_2. The appreciable adsorption of I^- anions on $BiVO_4$ particles is undoubtedly responsible for the efficient oxidation of I^- to IO_3^- (or I_3^-), which is thermodynamically more favorable than water oxidation, by photogenerated holes on $BiVO_4$ and for completely suppressing oxidation of water to O_2 (Figure 12b).

The rate of O_2 evolution over Pt–WO_3 gradually decreased and became almost zero after 30 h of photoirradiation (Figure 18) under basic conditions, accompanied by a slight color change in the solution from transparent to cloudy pale yellow. It is known that WO_3 is chemically unstable under alkaline conditions. The deactivation of the Pt–WO_3 photocatalyst under basic conditions is undoubtedly due to the chemical dissolution of the WO_3 surface during the reaction. As can be seen in the inset of Figure 18, the initial rate of O_2 evolution slightly increased with increasing pH of the solution. Although the highest O_2 evolution rate was obtained under basic conditions (pH 8.6), the O_2 evolution rate decreased with prolonged time, as described above.

We then used these photocatalysts (Pt–WO_3 and Pt–$BiVO_4$) as an O_2 evolution photocatalyst instead of rutile TiO_2, in the combination with Pt–anatase TiO_2 photocatalyst, in a neutral aqueous solution of NaI (40 mM, pH 6.5 without adjustment) under UV light irradiation. As shown in Table 1, the combination of Pt–TiO_2-A1 and Pt–WO_3 resulted in simultaneous evolution of H_2 and O_2 under UV light irradiation. Meanwhile, steady gas evolution was not observed by using the Pt–$BiVO_4$ as an O_2 evolution photocatalyst, combined with Pt–anatase

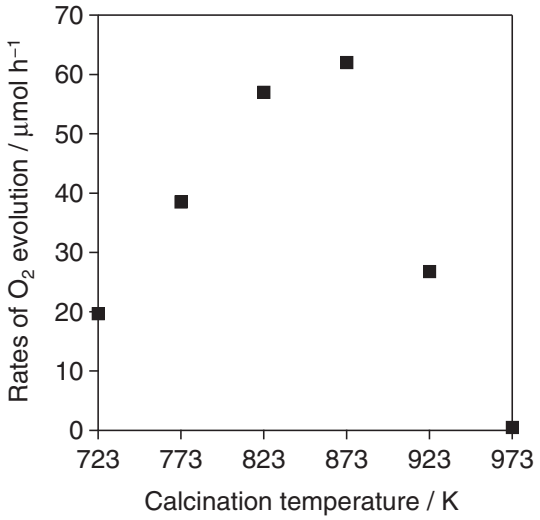

Figure 21. Dependence of rates of O_2 evolution over Pt(0.5 wt %)–WO_3 photocatalysts upon the calcination temperature after impregnation of $H_2[PtCl_6]$. The reaction was carried out in aqueous solution (250 mL) containing $NaIO_3$ (2 mM).

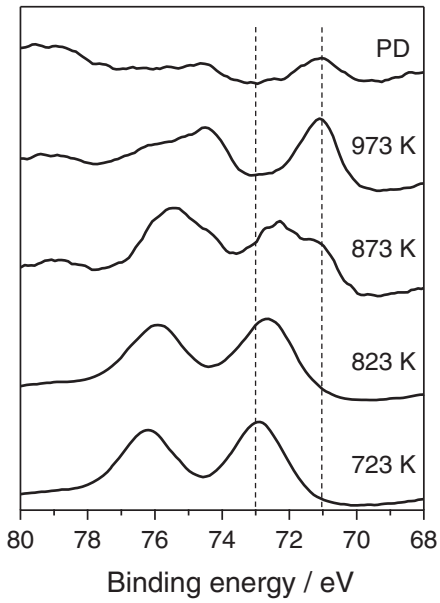

Figure 22. XPS spectra for Pt 4f of 0.5 wt % Pt-loaded WO_3 prepared by photodeposition (PD) and impregnation method with different calcination temperatures.

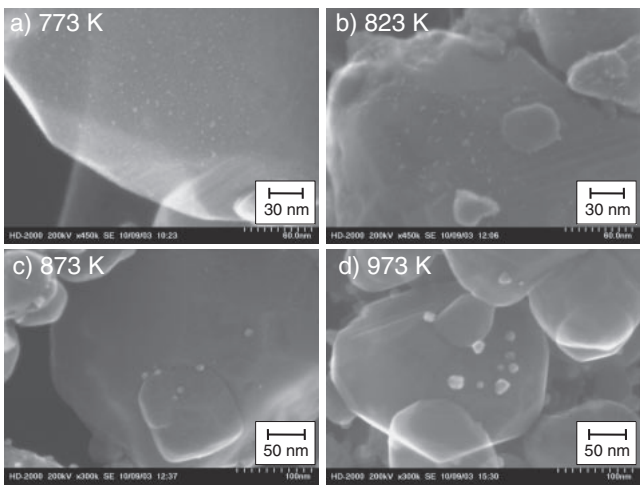

Figure 23. STEM images 0.5 wt % Pt-loaded WO_3 prepared by impregnation method with different calcination temperatures.

TiO_2. These results have shown that selective O_2 evolution in the presence of I^- anions is indispensable for the photocatalyst used as an O_2 evolution photocatalyst in the present water-splitting system.

3.2 Effect of Pt Loading on WO_3 upon O_2 Evolution in the Presence of the Electron Acceptor IO_3^-. The loading of cocatalyst, such as Pt or RuO_2, is indispensable for efficient O_2 evolution over the WO_3 photocatalyst using the IO_3^- anion as an electron acceptor, as described in a previous Section **3.1**. Given the fact that even bare WO_3 photocatalysts exhibit a relatively high activity for O_2 generation from water in the presence of other electron acceptors such as Ag^+ or Fe^{3+},[79–81] it appears that the Pt cocatalyst mainly serves to provide reduction sites that enable the multielectron reduction of IO_3^- to I^- (eq 3). Figure 21 shows the dependence of the rate of O_2 evolution over the Pt(0.5 wt %)–WO_3 photocatalyst upon calcination temperature after impregnation of $H_2[PtCl_6]$. The rate of O_2 evolution increased significantly with increasing calcination temperature from 723 to 823 K, and then decreased sharply above 873 K. It was confirmed that the calcination of a bare WO_3 in air up to 973 K had a negligible effect on the rate of O_2 evolution from water in the presence of the electron acceptor Ag^+ (not shown). The rate of O_2 evolution over the photodeposited Pt–WO_3 (ca. 5 μmol h^{-1}) was much lower than that over impregnated Pt–WO_3 samples. The significant effect of Pt loading was indicative of the different physicochemical properties of the Pt on WO_3. The electronic state of the loaded Pt species on WO_3 was thus investigated by XPS. Figure 22 shows XPS spectra for Pt 4f in 0.5 wt % Pt-loaded samples prepared by photodeposition (PD) and impregnation at different temperatures. The photodeposited sample exhibited a main peak with a binding energy of ca. 71.0 eV, which was assignable to $4f_{7/2}$ electrons of metallic Pt (Pt^0). The impregnated sample prepared at low temperature (723–823 K) exhibited a main peak with a binding energy of ca. 73.0 eV, which was assignable to the Pt(II) species. The samples prepared at higher temperatures (>873 K) were found to contain metallic Pt species, as well as Pt(II) species. Figure 23 shows STEM images of Pt-loaded WO_3 samples prepared by impregnation of $H_2[PtCl_6]$ followed by calcination in air at different temperatures. Highly dispersed fine particles (2–5 nm) were observed on the Pt–WO_3 sample prepared at 773 K. The XPS results strongly suggested that these were platinum oxide (PtO) particles that contained Pt(II) species. The fine particles gradually coarsened at higher calcination temperatures of up to 873 K, and then aggregated to form noticeably larger particles (≈20 nm) at 973 K. The increase in the O_2 evolution rate with temperature from 723 to 823 K is certainly due to the improved interface between WO_3 and PtO particles, which enables efficient electron transport from WO_3 to PtO. Calcination at 973 K resulted in relatively large particles of metallic Pt, as

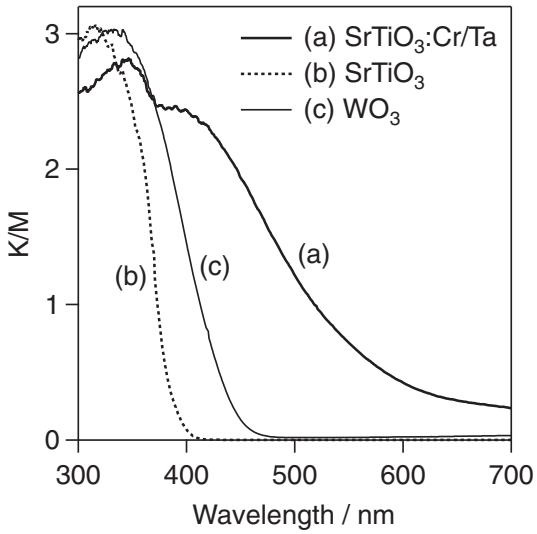

Figure 24. Diffused reflectance spectra of $SrTiO_3$:Cr/Ta (a), $SrTiO_3$ (b), and WO_3 (c).

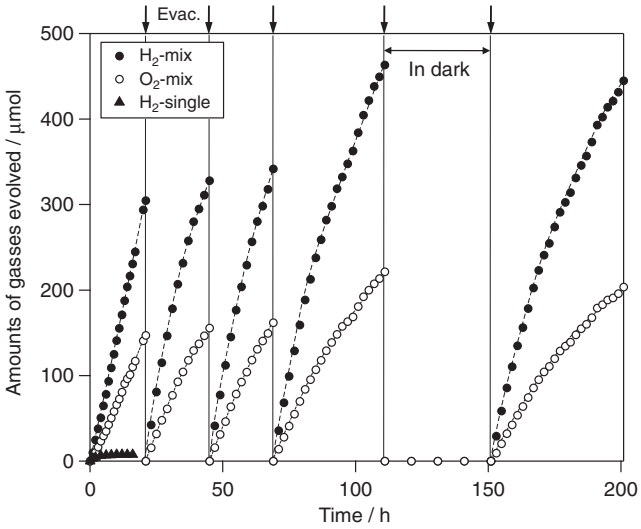

Figure 25. Time course of photocatalytic evolution of H_2 and O_2 using a mixture of Pt(0.3 wt %)–$SrTiO_3$ (Cr, Ta 4 mol % doped) and Pt(0.5 wt %)–WO_3 photocatalysts suspended in 5 mM of NaI aqueous solution (pH 6.5 without adjustment) under visible light irradiation ($\lambda > 420$ nm). Triangles indicate H_2 evolution using Pt–$SrTiO_3$:Cr/Ta alone.

confirmed by STEM and XPS, and negligibly low O_2 evolution rates. These results suggested that the decrease in O_2 evolution rate above 873 K is due to both the aggregation of cocatalyst particles and the change in the chemical state of cocatalyst particles from platinum oxide (PtO) to platinum metal (Pt). Considering the fact that the photodeposited Pt–WO_3 samples, which were loaded with highly dispersed Pt metal particles, showed a much lower activity for O_2 evolution (ca. 5 μmol h^{-1}), it appears that the chemical composition of Pt species affected the efficiency of O_2 evolution to a greater extent in the presence of the electron acceptor IO_3^-. These results strongly suggested that PtO is a more favorable cocatalyst for IO_3^- reduction than Pt metal. It is well known that Pt nanoparticles act as highly efficient catalyst for O_2 reduction. We have recently demonstrated that photodeposited Pt–WO_3 photocatalysts showed a highly efficient activity for oxidative decomposition of various organic compounds through the multielectron reduction of O_2 molecules on Pt nanoparticles.[177,178] Therefore, one possible reason for the low activity of WO_3 samples loaded with a Pt metal cocatalyst is competitive reduction of O_2 molecules on the Pt metal surface alongside the reduction of IO_3^-.

3.3 Simultaneous Evolution of H_2 and O_2 under Visible Light Irradiation Using a Combination of $SrTiO_3$:Cr/Ta and WO_3 Photocatalysts. A visible-light-driven water-splitting system was then constructed by employing the same strategy as in the TiO_2 system. $SrTiO_3$ codoped with Cr and Ta ($SrTiO_3$:Cr/Ta) was found to be active photocatalyst for both H_2 and IO_3^- production from an aqueous NaI solution under visible light irradiation ($\lambda > 410$ nm).[75–77] This photocatalyst was originally developed by Kudo et al. and has a reasonably high activity for H_2 evolution from water under visible light irradiation in the presence of methanol as a sacrificial electron donor.[118] The diffuse reflectance spectra of WO_3, pristine $SrTiO_3$, and $SrTiO_3$:Cr/Ta are presented in Figure 24. The codoping of Cr and Ta into $SrTiO_3$ created broad absorption in the visible region up to ca. 700 nm. The Pt-loaded $SrTiO_3$:Cr/Ta showed an appreciable H_2 evolution under the light irradiation with wavelength shorter than ca. 550 nm, while the absorption longer than 550 nm, which is derived from Cr^{6+} species, rarely contributes to photocatalytic H_2 evolution.[118,119] Although the rate of H_2 evolution over only the Pt–$SrTiO_3$:Cr/Ta photocatalyst decreased remarkably with irradiation time due to the backward reaction (re-reduction of IO_3^- to I^- by photoexcited electrons), using both Pt–$SrTiO_3$:Cr/Ta and Pt–WO_3 photocatalysts resulted in simultaneous evolution of H_2 and O_2 (initial H_2 rate: 16 μmol h^{-1}, initial O_2 rate: 8 μmol h^{-1}) from an aqueous NaI solution under visible light irradiation ($\lambda > 410$ nm), as shown in Figure 25. The reaction proceeded with no noticeable deactivation, even for long irradiation times. The total amount of H_2 gas evolved reached ca. 1.9 mmol, exceeding the stoichiometric amounts of the photocatalysts ($SrTiO_3$:Cr/Ta: 1.1 mmol, WO_3: 1.4 mmol) and I^- (1.25 mmol) in the solution. The reaction mechanism is undoubtedly the same as that of the Pt–anatase TiO_2/rutile TiO_2 combined system. That is, H_2 and IO_3^- production proceeded over the Pt–$SrTiO_3$:Cr/Ta photocatalyst. At the same time, re-reduction of IO_3^- to I^- and oxidation of water to O_2 occurred over the Pt–WO_3 photocatalyst under visible light irradiation. This was the first demonstration of water splitting into H_2 and O_2 under visible light irradiation. It represents one of the most important technical breakthroughs in the field of photocatalytic water splitting.

Figure 26 shows the dependence of gas evolution rates over the combination of Pt–$SrTiO_3$:Cr/Ta and Pt–WO_3 photocatalysts upon the amount of dopants into $SrTiO_3$ material. In all cases, the equal molar amount of Ta^{5+} to Cr^{3+} was codoped into $SrTiO_3$ in place of Ti^{4+} cations, in order to compensate the charge balance among Ti^{4+}, Cr^{3+}, and Ta^{5+}.[118] The rates of gas evolution increased with the increasing amount of dopants up to 4 mol %, while further doping lowered the efficiency. Kudo

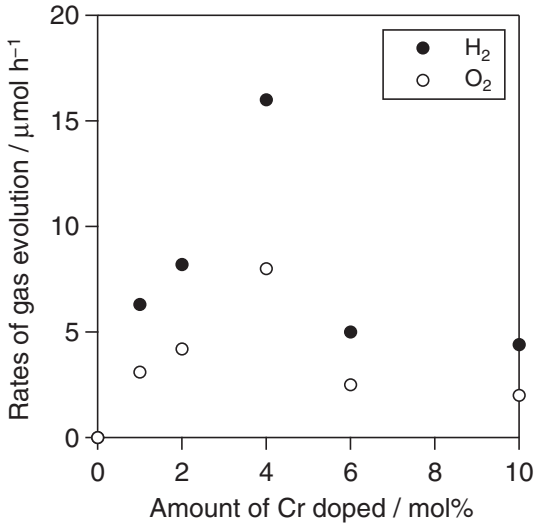

Figure 26. Dependence of rates of gas evolution over a mixture of Pt–$SrTiO_3$ (Cr, Ta doped) and Pt–WO_3 photocatalysts upon the amount of chromium.

and co-workers reported a similar trend for H_2 evolution over Pt–$SrTiO_3$:Cr/Ta photocatalyst in the presence of sacrificial electron donor methanol.[118] The increase in the doping amount of Cr^{3+} enhances visible light absorption, however, it also works as a recombination center between photogenerated electrons and holes. Consequently, volcano-type dependence on doping amount was obtained.

3.4 Summary. Overall water splitting under visible light was demonstrated for the first time through two-step photoexcitation between Pt–$SrTiO_3$:Cr/Ta and Pt–WO_3 in the presence of an iodate–iodide (IO_3^-/I^-) shuttle redox mediator. Photocatalytic O_2 evolution proceeded at a steady rate over Pt–WO_3, continuing until almost all IO_3^- anions in the solution were reduced to I^-, certainly due to the distinctly different adsorption properties between IO_3^- and I^- on WO_3 surface. This high selectivity of Pt–WO_3 photocatalyst for the forward reactions (IO_3^- reduction and water oxidation) is perfectly useful to construct an overall water-splitting system in combination with another photocatalyst for H_2 evolution, even if it has low selectivity for the H_2 evolution. For example, the H_2 evolution over the Pt–$SrTiO_3$:Cr/Ta photocatalyst alone readily terminated due to the significant backward reaction, re-reduction of IO_3^- on the Pt cocatalyst, even with a quite small amount of IO_3^- accumulated in the solution. The coexistence of Pt–WO_3 photocatalyst, which can efficiently consume IO_3^-, maintains a very low concentration of IO_3^- during the reaction, effectively suppressing the undesirable backward reaction (IO_3^- reduction to I^-) over the Pt–$SrTiO_3$:Cr/Ta photocatalyst, and thus resulting in the sustained H_2 evolution. Although WO_3 material has one serious disadvantage, instability under basic conditions, the excellent properties as an O_2 evolution photocatalyst are quite useful to construct overall water splitting through two-step photoexcitation via redox cycle between IO_3^-/I^-. Therefore, the Pt–WO_3 photocatalyst is mainly used as an O_2 evolution photocatalyst in combination with other H_2 evolution photocatalysts such as oxynitrides or dye-sensitized oxides, which will be discussed in later sections.

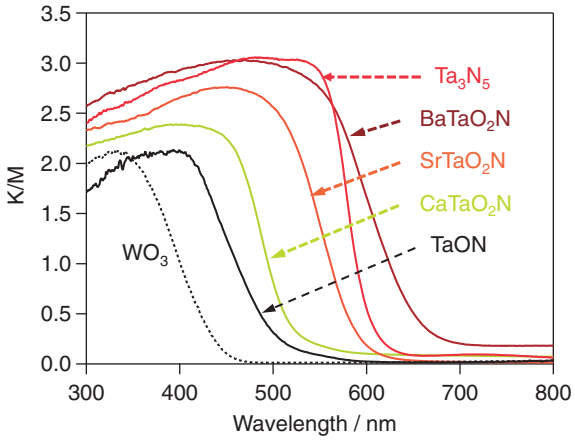

Figure 27. Diffused reflectance spectra of various (oxy)nitrides and WO_3.

4. Application of Tantalum Oxynitride Photocatalysts to a Z-Scheme with IO_3^-/I^- Redox Mediator[150,153–155,157–160]

As described above, photocatalytic water splitting under visible light has been achieved by using a doped oxide, $SrTiO_3$:Cr/Ta, as the H_2 photocatalyst together with WO_3. However, few oxide semiconductors have both a high visible light absorption and a sufficiently high potential for H_2 evolution, because of the highly positive valence bands of oxides, which are mainly formed by O 2p orbitals. Domen et al. have reported that some oxynitride (e.g., TaON,[133] $BaTaO_2N$,[136] and $LaTiO_2N$[132,134]) or nitride (e.g., Ta_3N_5[92]) powder photocatalysts exhibit activity for H_2 production from water in the presence of a sacrificial electron donor such as methanol under visible light irradiation. Because N 2p orbitals have much more negative energy levels than O 2p orbitals, the tops of the valence bands of oxynitrides and nitrides are more negative than those of the corresponding oxide. For example, the potential energies of the tops of the valence bands increase in the order Ta_2O_5 (3.6 V) < TaON (2.0 V) < Ta_3N_5 (1.6 V vs. NHE).[179] On the other hand, the bottoms of the conduction bands of these (oxy)nitrides (TaON and Ta_3N_5) consist of predominantly empty orbitals of tantalum, resulting in similar energy levels to that of the corresponding metal oxide (Ta_2O_5) in the range −0.3 to −0.5 V (vs. NHE), which are suitable for H_2 production.[179] As shown in Figure 27, these (oxy)nitrides can absorb a wider wavelength range of visible light due to their narrower band-gap energies than visible-light-responsive oxides such as WO_3. Consequently, these (oxy)nitride materials are considered to be promising H_2 photocatalysts for two-step (Z-scheme) water-splitting systems. In this section, the application of tantalum oxynitride (e.g., TaON, $ATaO_2N$) photocatalysts to H_2 evolution in a Z-scheme with IO_3^-/I^- redox mediator will be reviewed. Additionally, the application of (oxy)nitrides to O_2 evolution will be also reviewed in the later part.

4.1 Application of Simple Tantalum Oxynitride (TaON) to H_2 Production. Photocatalytic H_2 production was found to proceed over the Pt-loaded TaON samples in an aqueous solution containing I^- anions as a reversible electron donor under visible light ($\lambda > 410$ nm), as shown in Figure 28. The

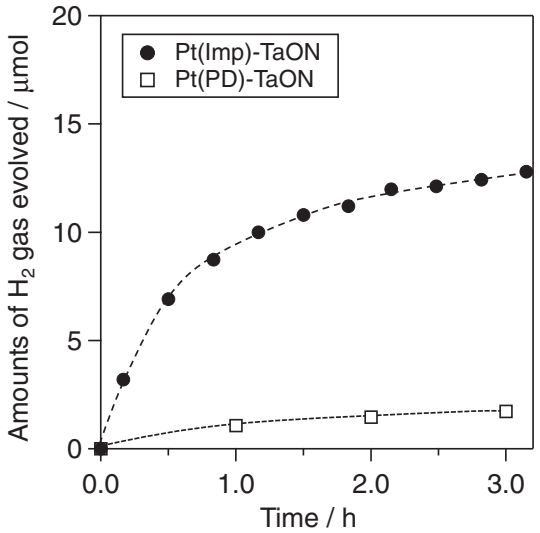

Figure 28. Time course of photocatalytic evolution of H_2 using a Pt(0.3 wt %-Imp)–TaON or Pt(0.3 wt %-PD)–TaON photocatalyst (0.2 g) suspended in a 10-mM aqueous NaI solution (pH 6.5 without adjustment) under visible light ($\lambda > 410$ nm).

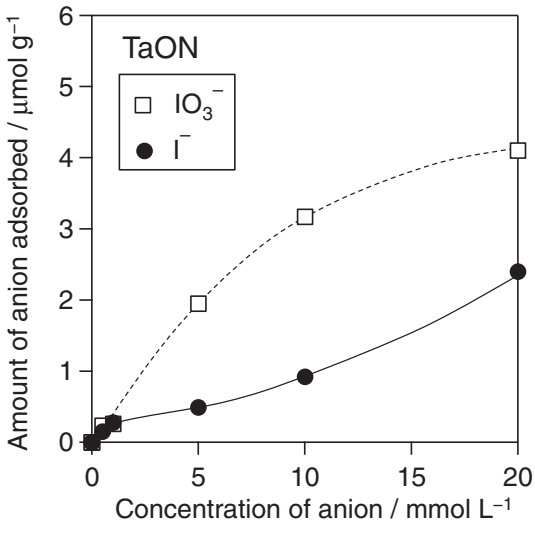

Figure 29. Adsorption properties of iodate (IO_3^-) and iodide (I^-) anions on TaON photocatalyst powder.

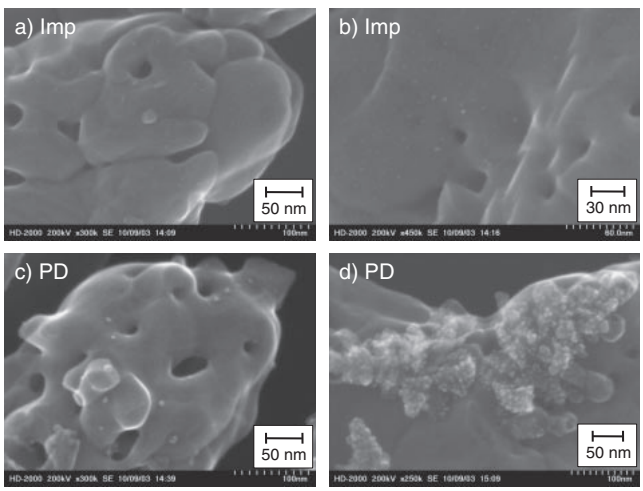

Figure 30. STEM images 0.3 wt % Pt-loaded TaON prepared by impregnation (a, b), and by photodeposition (c, d).

production of IO_3^- anions in the solution was also confirmed. Neither O_2 nor N_2 were evolved during the reaction. It has been reported that some (oxy)nitride materials suffer from self-oxidative decomposition,[132,134] whereby nitrogen anions (N^{3-}) are oxidized to N_2 by photogenerated holes:

$$2N^{3-} + 6h^+ \rightarrow N_2 \quad (10)$$

Although such self-oxidative generation of N_2 was observed when TaON was used for O_2 evolution from water in the presence of Ag^+ electron acceptor,[133] no N_2 gas was evolved in the presence of I^- anions. These results indicate that the I^- anions acted as effective electron donors for the TaON photocatalyst, which consequently suppressed the self-oxidative deactivation of the TaON surface. The rate of H_2 evolution gradually decreased and became almost zero after 3 h of photoirradiation, due to the backward reaction (re-reduction of IO_3^-). Both IO_3^- and I^- ions adsorbed on the surface of the TaON photocatalyst powder, as seen in Figure 29, while IO_3^- showed a higher adsorptivity than I^- at higher concentrations. The appreciable adsorption of the I^- ions on TaON clearly enabled the efficient oxidation of I^- to IO_3^- by the photogenerated holes on the TaON photocatalyst and effectively suppressed the self-oxidative deactivation of TaON. However, the competitive adsorption of IO_3^- anions on TaON caused a significant backward reaction (reduction of IO_3^- to I^-, instead of H_2 production) over the Pt–TaON photocatalyst in the presence of both IO_3^- and I^- anions, lowering the rate of H_2 evolution.

As can be seen in Figure 28, the Pt-loaded TaON sample prepared by photodeposition (Pt(PD)–TaON) showed a much lower activity than that prepared by impregnation (Pt(Imp)–TaON) with H_2 reduction at 473 K. Because photodeposition generally results in selective dispersion of metal nanoparticles (e.g., Pt) on the reduction sites of the photocatalyst, highly active photocatalysis is expected based on efficient electron transfer from the semiconductor to the metal nanoparticles. Although such photodeposition method is quite effective in activating oxide semiconductors for water reduction and thus has consequently been utilized in many oxide photocatalyst systems, the photodeposition could not afford significant improvement in the H_2 evolution on TaON. Figure 30 shows STEM images of Pt-loaded TaON samples. In the photodeposited sample, relatively large Pt particles (≈10 nm) were poorly dispersed on the TaON particles (Figure 30c), with some large aggregates in part (Figure 30d). On the other hand, Pt nanoparticles smaller than 5 nm were highly dispersed on the impregnated TaON samples (Figures 30a and 30b). The impregnation method allows a higher dispersion of Pt nanoparticles on the surface of TaON particles, which in turn results in a higher rate of H_2 evolution.

Figure 31 shows the dependence of the initial rates of H_2 evolution over the Pt(0.3 wt %)–TaON photocatalyst prepared by impregnation upon (a) the NaI concentration at pH 6.5, and

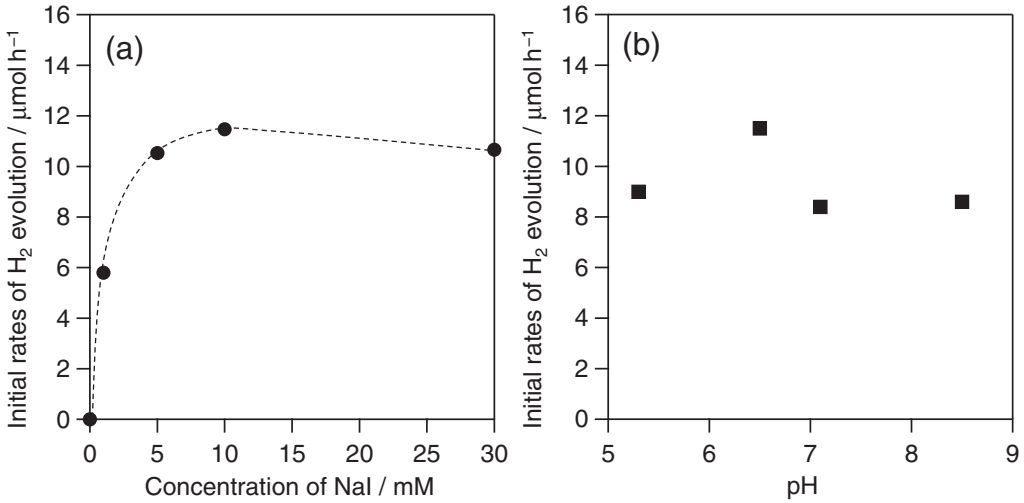

Figure 31. Dependence of rates of H_2 evolution over Pt(0.3 wt %-Imp)–TaON photocatalyst upon (a) the NaI concentration at pH 6.5, and (b) the pH value of a 10-mM aqueous NaI solution.

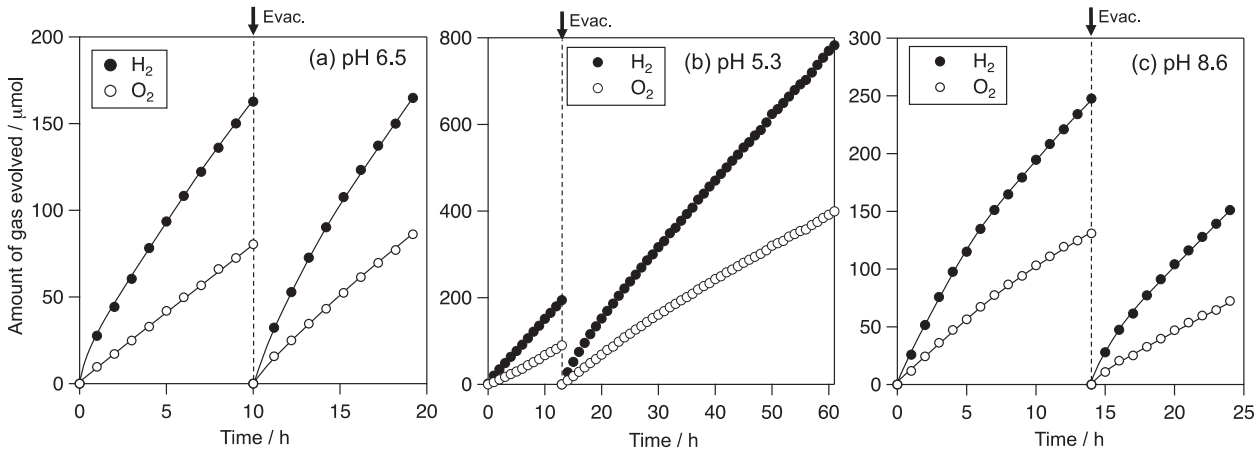

Figure 32. Time courses of gas evolution over a mixture of Pt(0.3 wt %)–TaON and Pt(0.5 wt %)–WO_3 photocatalysts under visible light irradiation from aqueous solution of NaI (5 mM) with pH 6.5 (a), 5.3 (b), and 8.6 (c).

(b) the pH value of a 10-mM aqueous NaI solution. The rate of H_2 evolution increased with NaI concentration up to 10 mM, and then almost saturated. The increase in the H_2 evolution rate was undoubtedly due to the enhancement in the reaction between photogenerated holes and the I^- electron donor. The rate of H_2 evolution over Pt–TaON was somewhat pH-independent from 5 to 8, while the rate of H_2 evolution was slightly lowered by the addition of a phosphate buffer.

4.2 Water Splitting into H_2 and O_2 under Visible Light Irradiation Using a Combination of TaON and WO_3 Photocatalysts. Overall water splitting under visible light was also examined by combining the Pt–TaON photocatalyst with the Pt–WO_3 photocatalyst in the presence of an IO_3^-/I^- shuttle redox mediator. The Pt(0.3 wt %)–TaON sample was prepared by impregnation of $H_2[PtCl_6]$(aq) with H_2 reduction at 473 K, and used as the H_2 evolution photocatalyst. As for the WO_3 photocatalyst, 0.5 wt % of Pt was loaded with impregnation of $H_2[PtCl_6]$ followed by calcination in air at 823 K, whereby platinum oxide (PtO) cocatalyst particles were loaded on the WO_3. As shown in Figure 32a, the combination of the Pt(0.3 wt %)–TaON and Pt(0.5 wt %)–WO_3 photocatalysts resulted in simultaneous H_2 and O_2 evolution from an aqueous NaI solution (5 mM, pH 6.5 without adjustment) under visible light irradiation. No appreciable N_2 gas evolution was detected during the photoirradiation, and no gas evolution was observed in darkness. These results demonstrate that overall water splitting proceeds by a two-step photoexcitation mechanism combined with a redox cycle between the anions IO_3^- and I^-, as shown in Figure 33. The quantum efficiency for overall water splitting was determined to be ca. 0.5% at 420 nm under the same conditions as for Figure 32a. Simultaneous H_2 and O_2 evolution also proceeded at a steady rate in a weakly acidic solution (pH 5.3), as shown in Figure 32b. The reaction proceeded without notable deactivation even after 60 h of irradiation, and the total amount of H_2 gas evolved reached ca. 0.98 mmol, exceeding the stoichiometric amount of the photocatalysts (TaON, 0.95 mmol; WO_3, 0.86 mmol). By contrast, the rate of gas evolution gradually decreased with prolonged irradiation time when the reaction was carried out in a weakly basic solution, as shown in Figure 32c. This is definitely due to the deactivation of the Pt–WO_3 photocatalyst under basic conditions, as seen in Figure 18. Figure 34a shows the de-

pendence of the gas evolution rate (determined from total amount of gasses evolved in 5 h) on the pH of reaction solution, in which the rate of gas evolution increased with pH. As seen in Figure 31b, the rate of H_2 evolution over Pt–TaON alone was barely affected by the pH. By contrast, the rate of O_2 evolution over the Pt–WO_3 photocatalyst alone increased with pH (Figure 18). Thus, it appears that the overall efficiency of this combination was dominantly affected by the efficiency of the O_2 evolution system (Pt–WO_3 photocatalyst) under the present reaction conditions. The rate of water splitting over the combination of Pt(0.3 wt %)–TaON and Pt(0.5 wt %)–WO_3 was measured in aqueous solutions (pH ≈6.5, without adjustment) with different NaI concentrations. The rate of gas evolution increased with I^- concentration up to 5 mM, decreasing significantly with further increase in concentration, as shown in Figure 34b. The enhancement of the gas evolution rate is undoubtedly due to the promotion of H_2 evolution on the Pt–TaON photocatalyst by the addition of the I^- electron donor. However, the addition of excess NaI had a negative effect on the overall water-splitting reaction. The decrease in the gas evolution rate is due to the competitive oxidation of I^- over the Pt–WO_3 photocatalyst, which decreases the rate of O_2 evolution as indicated by the results in Figure 19. The significant decrease in gas evolution rates for NaI concentrations above 10 mM again suggested that the overall efficiency in the present system was affected to a greater extent by the efficiency of the O_2 evolution system (Pt–WO_3 photocatalyst). It should be noted that the ratio of the amount of evolved O_2 to H_2 was not stoichiometric ($O_2/H_2 = 0.5$) at I^- concentrations above 10 mM, as shown in Figure 34b. The accumulation of I_3^- anions was confirmed at the end of reactions at high NaI concentrations of above 10 mM. Such accumulation of I_3^- was also observed for the O_2 evolution reaction over Pt–WO_3 alone in the presence of the IO_3^- electron acceptor under a high concentration of I^- (reactions shown in Figure 19). These results suggested that some of the photogenerated holes in Pt–WO_3 oxidized I^- to I_3^- (eq 8), alongside the oxidation of I^- to IO_3^- (eq 5). As described in Section **2.1**, I_3^- is not as efficient an electron acceptor as IO_3^- for oxide semiconductors such rutile TiO_2. It is therefore speculated that photoexcited electrons on Pt–WO_3 are unable to reduce I_3^- effectively, resulting in suppressed O_2 evolution and an appreciable deviation in the O_2/H_2 ratio. The I_3^- ions are thought to originate from the oxidation of I^- by holes (eq 8) over Pt–TaON, not only over Pt–WO_3. Distinguishing between these two sites for I^- oxidation is difficult. Given the fact that IO_3^- was mainly produced over Pt–TaON even in the solution with high NaI concentration, it appears that I_3^- production mainly occurred over Pt–WO_3. Although such accumulation of I_3^- can be prevented by using an alkaline solution at a pH above 9, given the spontaneous disproportionation of I_3^- into IO_3^- (eq 9), we could not apply alkaline conditions because of the instability of the WO_3 photocatalyst. Although the

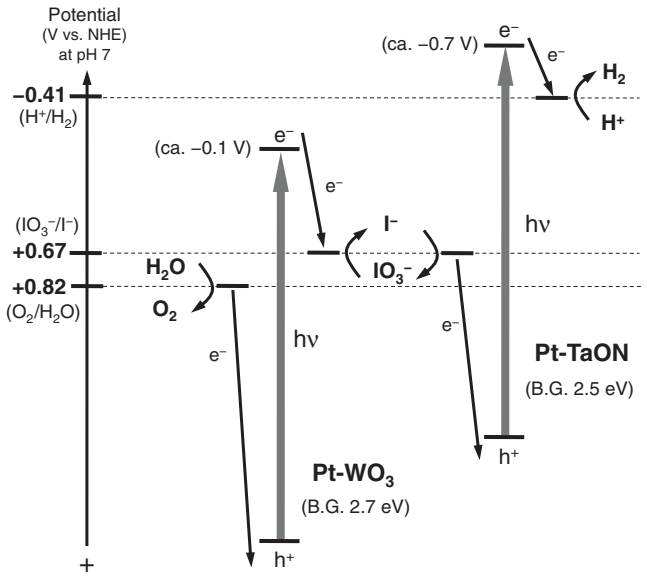

Figure 33. Energy diagram for overall water splitting over Pt–TaON and Pt–WO_3 with an IO_3^-/I^- shuttle redox mediator.

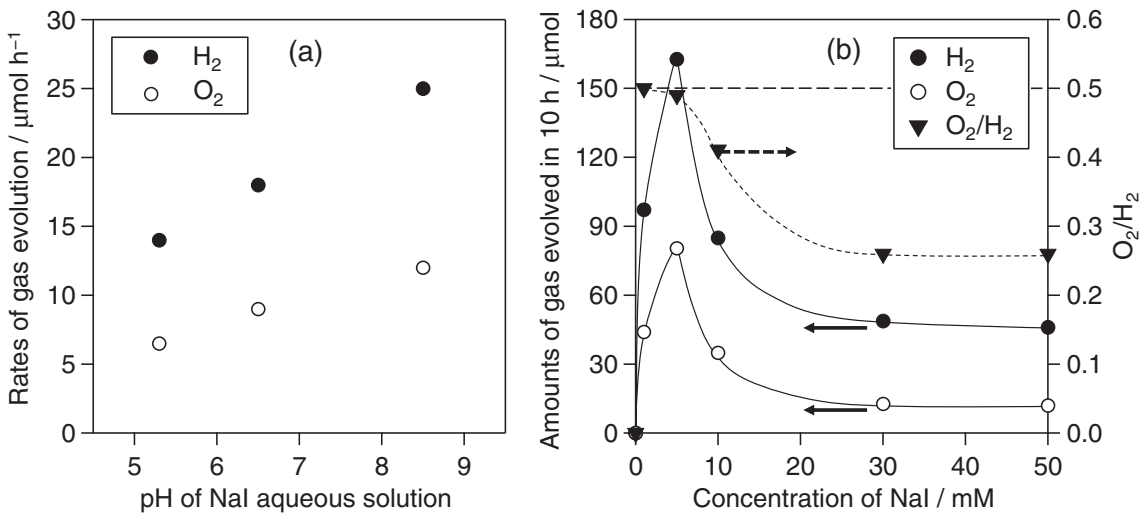

Figure 34. Dependence of rates of gas evolution a mixture of Pt(0.3 wt %)–TaON and Pt(0.5 wt %)–WO_3 photocatalysts under visible light irradiation upon (a) the pH value of NaI solution (NaI: 5 mM), and (b) upon the concentration of NaI aqueous solution (pH 6.5).

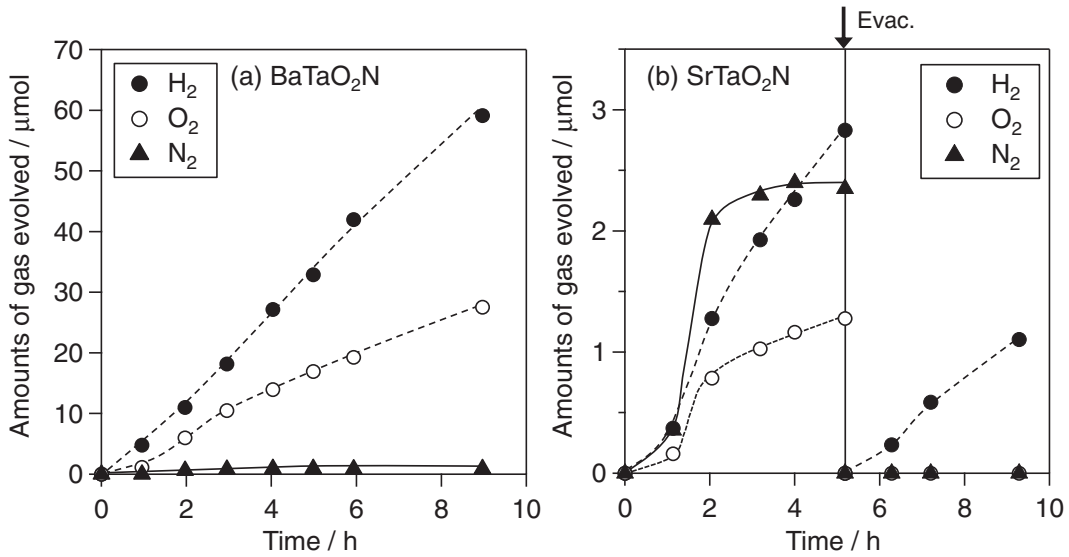

Figure 35. Time courses of H_2 and O_2 evolution over a mixture of Pt–WO_3 and (a) Pt–$BaTaO_2N$, (b) Pt–$SrTaO_2N$ under visible light ($\lambda > 410$ nm) in the presence of 5 mM NaI (Pt(0.3 wt %)–$ATaO_2N$, 0.1 g, Pt(0.5 wt %)–WO_3, 0.1 g).

predominant factor leading to the selectivity in I^- oxidation over photocatalysts remains unclear and requires further investigation, excessively high concentrations of I^- clearly decrease the efficiency for the overall water-splitting reaction. These results indicated that the concentration of the redox is a significant factor determining the efficiency of the overall reaction in the two-step water-splitting system using a redox couple. This significant influence of the redox concentration on overall efficiency basically results from the occurrence of backward reactions over both the H_2 and O_2 evolution photocatalysts. Therefore, controlling the reaction selectivity toward the forward reactions, H_2 evolution and O_2 evolution, is indispensable for achieving highly efficient water splitting based on two-step photoexcitation with redox mediators.

Although the (Pt–TaON)/(Pt–WO_3) system for water splitting had an apparent quantum yield of only 0.4% at 420 nm,[150] surface modification of TaON with ZrO_2 significantly increased the apparent quantum yield to 6.3% at 420 nm.[158] This is currently the highest reported apparent quantum yield for a nonsacrificial visible-light-driven water-splitting system. This high performance is at least partly due to suppression of electron–hole recombination in ZrO_2/TaON, which results from moderation of the n-type semiconducting character of TaON by the formation of a composite with ZrO_2.[158] Although (oxy)nitrides have previously been thought to have relatively low activities for H_2 evolution for water splitting, these results clearly demonstrate that they are very promising for water splitting after appropriate surface modification and optimization of the reaction conditions.

4.3 Water-Splitting System Using $BaTaO_2N$ Photocatalysts Responsive to Longer Wavelength up to 660 nm. Three mixed tantalum oxynitrides, $ATaO_2N$ (A = Ca, Sr, and Ba), prepared by heating amorphous $A_2Ta_2O_7$ under NH_3, were also applied in a two-step photoexcitation water-splitting system as a photocatalyst for H_2 evolution. These oxynitride photocatalysts enabled the Z-scheme to harvest visible light over a wide wavelength range. As shown in Figure 27, these tantalum oxynitrides with perovskite structure can absorb a wider wavelength range of visible light than visible-light-responsive oxides such as WO_3. Interestingly, the absorption edges of $ATaO_2N$ shift to longer wavelengths with increasing ionic radius of A^{2+} (Ca^{2+}: 1.34 Å; Sr^{2+}: 1.44 Å; Ba^{2+}: 1.61 Å).[136] All of the Pt-loaded $ATaO_2N$ samples were confirmed to exhibit photocatalytic activity for H_2 evolution from water under visible light irradiation in the presence of methanol as a sacrificial electron donor, without detectable N_2 evolution due to self-oxidative decomposition. Although the Pt-loaded $CaTaO_2N$ and $BaTaO_2N$ were also demonstrated to be active for stable H_2 evolution in the presence of I^- as a reversible electron donor, Pt-loaded $SrTaO_2N$ was unable to produce H_2 stably in the presence of I^- due to the self-oxidative decomposition accompanied by N_2 release. The combination of Pt–$BaTaO_2N$ and Pt–WO_3 photocatalysts allowed simultaneous H_2 and O_2 evolution from NaI aqueous solution under visible light at a close to stoichiometric ratio (H_2:O_2 = 2:1), while a small degree of N_2 evolution was also observed as shown in Figure 35a. The combination of Pt–$CaTaO_2N$ and Pt–WO_3 also achieved steady H_2 and O_2 evolution. On the other hand, the use of Pt–$SrTaO_2N$ as H_2 evolution photocatalyst failed to split water stably (Figure 35b), undoubtedly due to the self-oxidative decomposition of $SrTaO_2N$ photocatalyst as mentioned above. At present, the reason for the greater instability of $SrTaO_2N$ compared to that of the other $ATaO_2N$ materials is unclear. However, judging from the stable production of H_2 over Pt–$SrTaO_2N$ from aqueous methanol solution without N_2 evolution, self-oxidative decomposition is likely to be promoted by the reaction of the $SrTaO_2N$ compositions with iodide (I^-) or iodate (IO_3^-). Based on the absorption spectrum of $BaTaO_2N$ (Figure 27), it is expected that H_2 evolution over Pt–$BaTaO_2N$ proceeds by the absorption of visible light at wavelengths up to 660 nm. For confirmation of this behavior, the dependence of H_2 evolution over Pt–$BaTaO_2N$ on the wavelength of irradiation in overall water-splitting reaction was examined by using two xenon illuminators (A and B) with

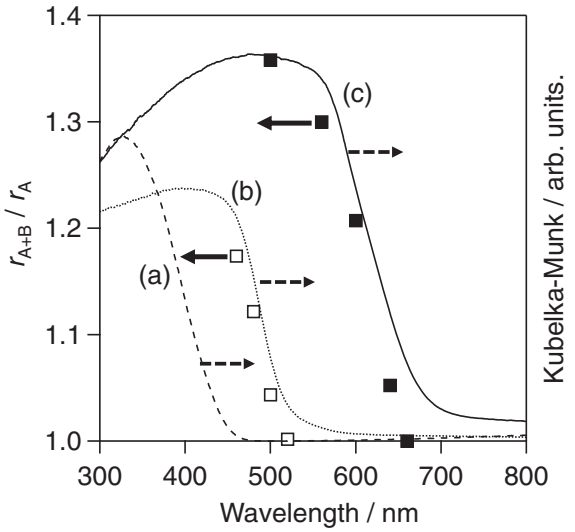

Figure 36. Variation in (r_{A+B}/r_A) ratio with cut-off wavelength of incident light (illuminator B) and absorption spectra for (a) WO_3, (b) $CaTaO_2N$, and (c) $BaTaO_2N$.

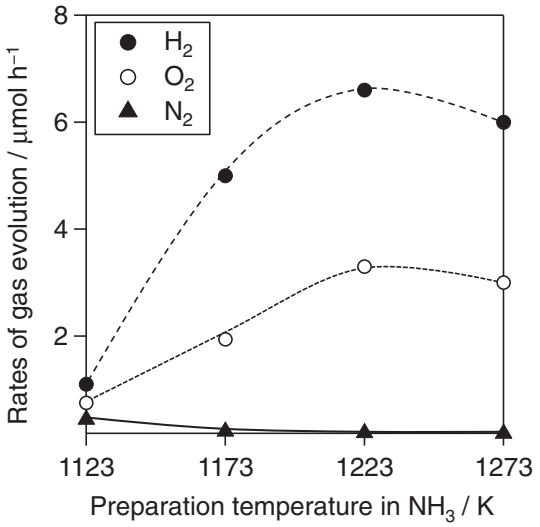

Figure 37. Preparation temperature dependence of photocatalytic activity of a combination of Pt–$BaTaO_2N$ and Pt–WO_3 under visible light ($\lambda > 410$ nm) in an I^-/IO_3^- shuttle redox mediated system.

different emission characteristics. Illuminator A emitted light at wavelengths longer than 420 nm (4.32×10^{22} photon h^{-1} at 420 nm $< \lambda <$ 660 nm), whereas illuminator B was fitted with a number of cutoff filters to produce only light with wavelength longer than 500 nm (2.54×10^{22} photon h^{-1} at 500 nm $< \lambda <$ 660 nm). The illuminator B was designed to excite $BaTaO_2N$ but not WO_3 (absorption edge, ca. 450 nm). Figure 36 plots the ratio of the total evolution rate (r_{A+B}) to that due to illuminator A alone (r_A) as a function of the cutoff wavelength of illuminator B. Data for Pt–$CaTaO_2N$ (adsorption edge, 520 nm) combined with Pt–WO_3 is also shown for comparison. In the case of $BaTaO_2N$, a ratio of 1.36 was obtained with the 500 nm cutoff wavelength for illuminator B, indicating that the H_2 evolution rate over Pt–$BaTaO_2N$ was enhanced by increasing the total flux of incident photons, leading to an increase in the overall reaction rate. The degree of enhancement of H_2 evolution (r_{A+B}/r_A) decreased with increasing cutoff wavelength, eventually reaching unity, indicating no enhancement under additional irradiation at wavelength longer than 660 nm. For $CaTaO_2N$, the enhancement of H_2 evolution was observed at wavelength shorter than 520 nm, consistent with the absorption edge determined for $CaTaO_2N$. These results demonstrated that the absorption of $BaTaO_2N$ at wavelengths up to 660 nm indeed contributed to H_2 evolution in the overall water-splitting reaction. It represents the first example of a water-splitting system that effectively utilizes visible light at wavelengths longer than 600 nm for H_2 evolution.

Since these $ATaO_2N$ oxynitrides were prepared by heating amorphous $A_2Ta_2O_7$ under NH_3, the heating temperature significantly affected the activities of these photocatalysts. Figure 37 shows dependence of gas evolution rate over (Pt–$BaTaO_2N$)/(Pt–WO_3) on the preparation temperature of the $BaTaO_2N$ sample. The rate increased markedly with preparation temperature from 1123 to 1223 K, and slightly decreased at 1273 K. Although all the $BaTaO_2N$ samples prepared at above 1123 K indicated an XRD pattern corresponding to perovskite structure, the UV–vis diffused reflectance spectra displayed substantial change with increasing temperature. As shown in Figure 38, the $BaTaO_2N$ samples prepared at low temperatures (1123 and 1173 K) exhibited a monotonically increasing absorption at wavelengths longer than 700 nm. Such photoabsorption is known to be responsive to the presence of anion vacancies or reduced metal cation species in the semiconductor, where the available electron can readily be excited to empty conduction band levels by absorbing light at even low energies. Thus, the $BaTaO_2N$ samples prepared at low temperature are likely host anion vacancies or reduced metal species such as Ta^{4+}. Such anion

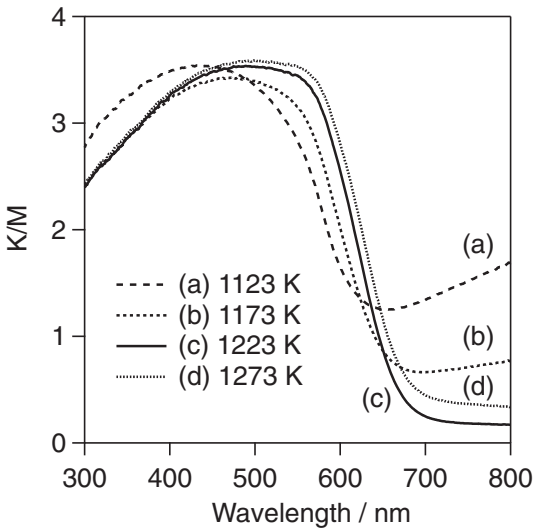

Figure 38. Diffuse reflectance spectra for $BaTaO_2N$ samples obtained by nitriding amorphous $Ba_2Ta_2O_7$ at (a) 1123, (b) 1173, (c) 1223, and (d) 1273 K for 20 h under NH_3 flow.

vacancies or reduced metal species are known to act as recombination centers for photogenerated carriers (i.e., electrons and holes). The presence of elevated densities of such sites can therefore be expected to degrade the photocatalytic activity of semiconductor materials. The increase in activity with preparation temperature certainly reflects the decrease in the density of such recombination centers in $BaTaO_2N$ as the temperature increases from 1123 to 1223 K. The rate of N_2 evolution decreased with increasing preparation temperature, suggesting self-oxidative decomposition is retarded by high crystallinity. As shown above, the presence of anion vacancies or reduced metal species significantly affects the photocatalytic activity of oxynitride photocatalysts. Therefore, decreasing such recombination centers will afford improved efficiency for water splitting, as we have recently demonstrated in a ZrO_2/TaON system.[158]

4.4 Application of Tantalum (Oxy)nitride Photocatalysts to O_2 Evolution in a Z-Scheme with IO_3^-/I^- Redox Mediator. Surface-modified (oxy)nitrides such as RuO_2–TaON and Ir/TiO_2–Ta_3N_5 can also be used as O_2 photocatalysts in a Z-scheme with an IO_3^-/I^- redox mediator. Because I^- anions react preferentially with photogenerated holes over TaON, the O_2 evolution over the bare TaON photocatalyst was completely suppressed even with a small amount of I^-. Thus, O_2-evolving cocatalysts such as RuO_2 and IrO_2 were loaded on the TaON surface to modify the selectivity of holes to oxidation of water. The loading of the RuO_2 cocatalyst on TaON was found to enhance O_2 evolution in the presence of the electron donor I^-, which enabled the RuO_2–TaON photocatalyst to be used as an O_2 photocatalyst in combination with Pt–TaON.[153] Structural analyses and (photo)electrochemical measurements revealed that the activity of RuO_2–TaON photocatalyst is strongly dependent on the generation of optimally dispersed RuO_2 nanoparticles, which simultaneously promote both the reduction of IO_3^- and oxidation of water.[160] We have recently demonstrated that the loading of IrO_2 cocatalyst on TaON electrode significantly improves both the photocurrent and the stability during photoirradiation.[180] The IrO_2 loading most likely resulted in efficient hole scavenging in the IrO_2 particles, preventing self-oxidation of the TaON surface. Modification of Ta_3N_5 by Ir metal and rutile TiO_2 particles also enhanced O_2 evolution.[157] The combinations (Pt–TaON)–(RuO_2–TaON) and (Pt–ZrO_2/TaON)–(Ir–TiO_2/Ta_3N_5) permitted water splitting over a wider wavelength range of visible light (TaON: 500 nm, Ta_3N_5: 600 nm) than systems using WO_3 (absorption edge of 450 nm) as the O_2 photocatalyst.[153,157,160]

4.5 Summary. A series of tantalum oxynitrides, TaON, $CaTaO_2N$, and $BaTaO_2N$, were successfully applied to the two-step overall splitting of water as a H_2 evolution photocatalyst through combination with Pt–WO_3 using IO_3^-/I^- as a shuttle redox mediator. The valence bands of these oxynitride materials are populated by N 2p orbitals mixed with O 2p, resulting in more negative valence band levels and smaller band gaps than conventional oxide semiconductors, allowing visible light-induced H_2 production from water. Indeed, Pt-loaded TaON, $CaTaO_2N$, and $BaTaO_2N$ were demonstrated to be active for H_2 evolution in the presence of I^- as an electron donor, whereas $SrTaO_2N$ was unable to produce H_2 stably due to self-oxidative decomposition accompanied by N_2 production. Photoabsorption by $BaTaO_2N$ was confirmed to extend to wavelengths as long as 660 nm, representing the first example of overall water splitting activated by light at wavelengths longer than 600 nm. Surface modification of (oxy)nitrides by cocatalyst for water oxidation enable these photocatalyst to be used as an O_2 photocatalyst. The use of RuO_2–TaON or Ir–TiO_2/Ta_3N_5 as O_2 evolution photocatalyst permitted water splitting over a wider wavelength range of visible light (TaON: 500 nm, Ta_3N_5: 600 nm) than systems using WO_3 (absorption edge of 450 nm). These results demonstrated the potential of a two-step water-splitting system for utilizing a broader band of the visible spectrum.

5. Robust Dye-Sensitized Water-Splitting System Workable under Visible Light with Two-Step Photoexcitation between Coumarin Dyes and WO_3 Photocatalysts[113]

As described above, water splitting under visible light has been achieved using various pairs of photocatalysts in the presence of an electron mediator IO_3^-/I^-. However, there are a limited number of suitable photocatalysts, primarily due to the difficulty in tuning the band levels of inorganic (particularly oxide) semiconductor photocatalysts. On the other hand, it is much easier to fine tune the energy levels (highest occupied molecular orbital (HOMO) and lowest unoccupied molecular orbital (LUMO)) of organic dyes than oxides, as has been demonstrated for dye-sensitized solar cells.[181–183] Studies on dye-sensitized solar cells have revealed that various organic dyes, including Ru complexes, possess both a sufficiently negative energy level (LUMO) for electron injection to the conduction band of TiO_2 and a sufficiently positive energy level (HOMO) to oxidize I^- to I_3^- in an organic solvent such as acetonitrile. Thus, using dye-sensitized n-type semiconductors (e.g., TiO_2) as a H_2 photocatalyst in the presence of an electron donor of I^- appears to a promising way to achieve efficient water splitting by utilizing a wider wavelength range of visible light. Figure 39 depicts the H_2 production processes over a dye-sensitized n-type semiconductor. An electron is excited from HOMO to LUMO by light absorption, injected into the conduction band of the semiconductor, and then consumed for H_2 production at a reduction site such as a Pt cocatalyst. The oxidized state of the dye is regenerated to the ground state by accepting an electron from an electron donor (Red). Although numerous studies have investigated dye-sensitized H_2 production in the presence of a sacrificial electron donor (e.g., tris(2-hydroxyethyl)amine),[98–108] there are few reliable dye-sensitized photocatalysts that are active for nonsacrificial H_2 production using a reversible electron donor such as I^-.[109–113] The instability of the oxidized state of a dye molecule in an aqueous medium is considered to be the main reasons why it is difficult to achieve steady H_2 production over dye-sensitized photocatalysts using I^- electron donors. We have found the stability of such organic dye molecules could be drastically improved by introducing an oligothiophene moiety between the donor and acceptor parts. Then we have demonstrated dye-sensitized water splitting into H_2 and O_2 under visible light irradiation for the first time using a simple organic dye molecule as a photosensitizer for H_2 evolution, a WO_3 photocatalyst for O_2 evolution, and an I_3^-/I^- redox couple as a shuttle redox mediator.[113]

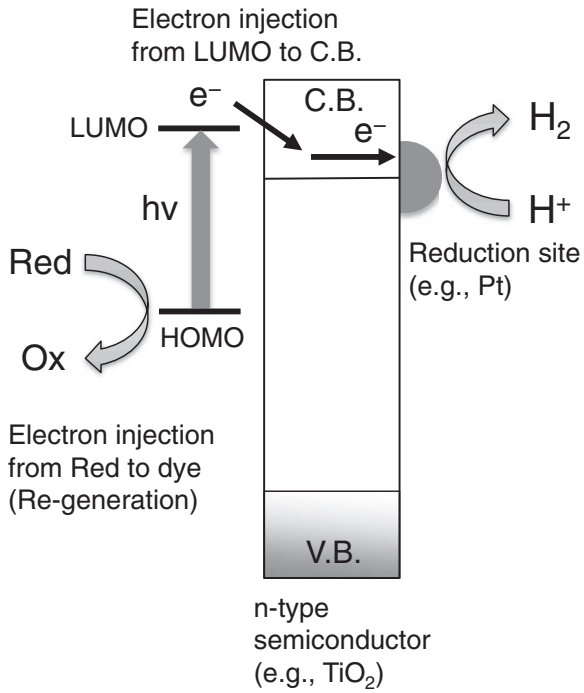

Figure 39. Conceptual scheme of H_2 production over dye-sensitized n-type semiconductor.

5.1 Significant Effect of Oligothiophene Moiety on the Stability of Dye Molecules in Water. We have been attempting to apply various kinds of organic dyes to H_2 production with I^- electron donor, and found that a coumarin dye (C-343) adsorbed onto Pt-loaded TiO_2 can generate H_2 from water in the presence of I^- electron donor.[111,112] Although the stability of coumarin C-343 was insufficient, it was revealed that introducing an oligothiophene moiety into the dye structure (between the donor and acceptor parts) significantly improved the stability of the oxidized state of the coumarin dyes in water and enabled the dye molecules to function as a robust sensitizer for H_2 production from water in the presence of an I^- electron donor. The structures of coumarin dyes used are shown in Figure 40. Figure 41 shows the *C–V* profiles of coumarin dyes in water and in a anhydrous AN solution containing 0.1 M $LiClO_4$ as a supporting electrolyte, along with their molecular structures. Since these dyes are barely soluble in an aqueous solution with a neutral pH, the CV measurements were carried out using nanoporous TiO_2 electrodes with the dyes adsorbed on them.[184] In all cases, a current peak was observed when an anodic potential of over +0.4 V (vs. reference) was applied, which indicates oxidation of the dye molecule (S) to an oxidized state (S^+). On the other hand, the reduction behavior strongly depended on the structure of the dye molecule. For NKX-2311, which does not have a thiophene ring, the reduction current peak

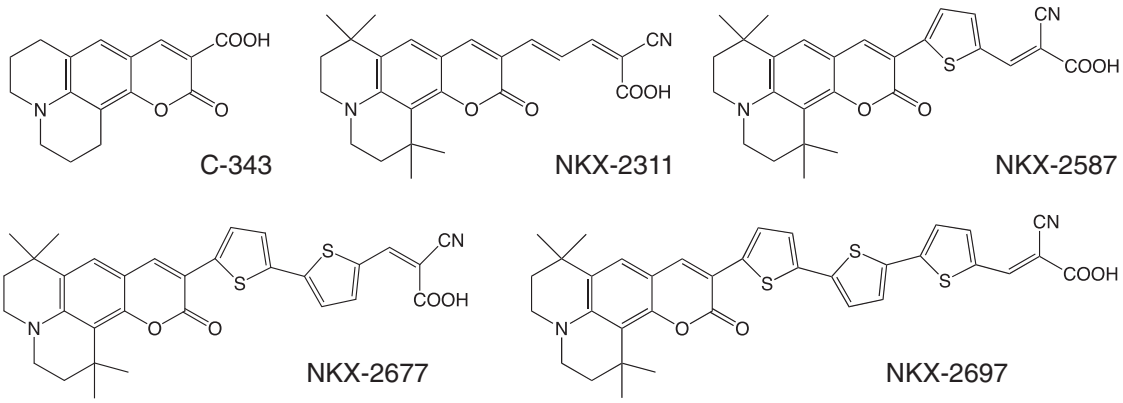

Figure 40. Molecular structures of coumarin dyes.

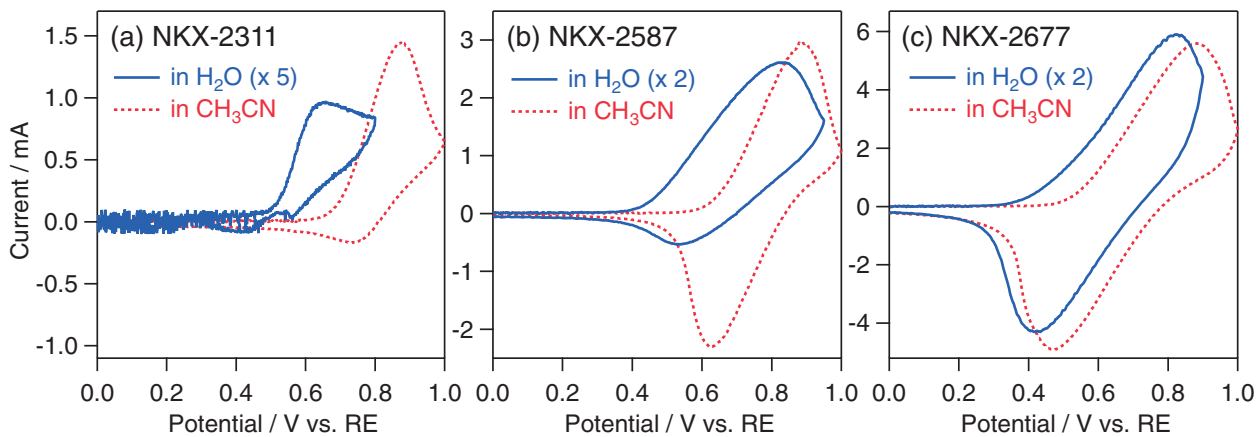

Figure 41. CV curves of coumarin dyes absorbed on a porous TiO_2 electrode in a dehydrated acetonitrile (AN) or aqueous solution containing 0.1 M $LiClO_4$ as a supporting electrolyte: the scan rate was 100 mV s^{-1}. Ag/AgCl in saturated aqueous NaCl solution and Ag/Ag^+ in 0.01 M $AgNO_3$ acetonitrile solution were used as a reference electrode in aqueous and AN solutions, respectively.

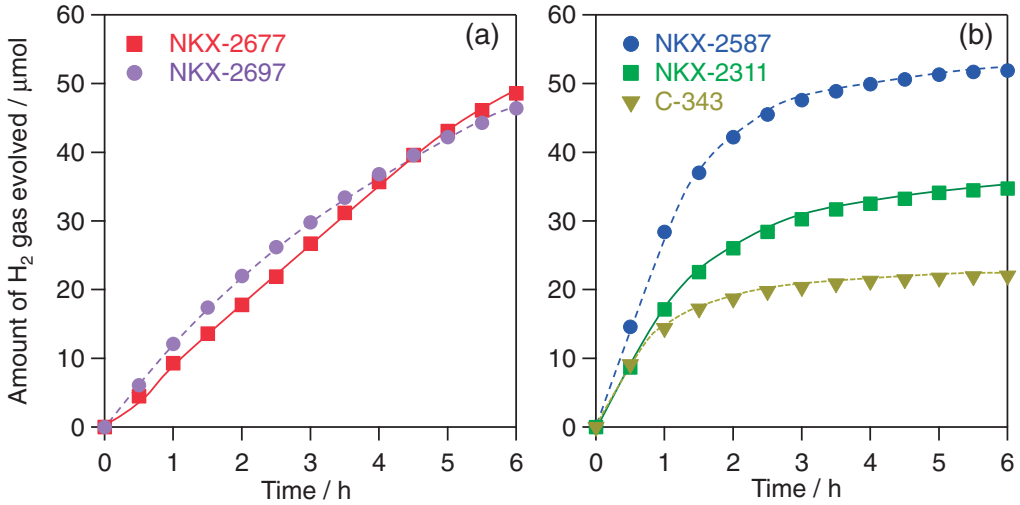

Figure 42. Time course of photocatalytic H_2 evolution by coumarin dye-adsorbed $Pt/H_4Nb_6O_{17}$ photocatalysts (50 mg) suspended in a 0.1 M aqueous KI solution (100 mL) under visible light ($\lambda > 410$ nm).

was much lower than the oxidation peak even in AN and no reduction peak was observed in water (Figure 41a). Although reversible behavior was observed for NKX-2587 in AN, the reduction current peak was much lower than the oxidation peak in water (Figure 41b). These results indicate that the oxidized state of these dyes (NKX-2311 and NKX-2587) reacted with H_2O irreversibly and formed inactive species. On the other hand, a reversible current peak was clearly observed in NKX-2677 during reverse cathodic scanning in both solvents (Figure 41c), indicating that, even in water, the oxidized state (S^+) has a relatively long lifetime and can be reduced back to its original state by accepting an electron during sweeping of the cathode potential. Based on the molecular structures of the coumarin dyes examined, it is concluded that thiophene moieties, (especially oligothiophene, which has more than two thiophene rings) play a significant role in stabilizing the oxidized states of the dyes in water.

5.2 Steady H_2 Evolution over Coumarin Dye with Oligothiophene Moiety in the Presence of I^- Electron Donor. Figure 42 shows the time course of H_2 evolution over coumarin dye-adsorbed $Pt–H_4Nb_6O_{17}$ (internally platinized $H_4Nb_6O_{17}$) photocatalysts suspended in aqueous potassium iodide (KI) solution under visible light irradiation. Steady H_2 evolution proceeded over the NKX-2677 and NKX-2697 dye-adsorbed photocatalysts (Figure 42a), and nearly the same amount of I_3^- anion as H_2 gas was detected in the solutions after the reaction in both cases (e.g., H_2: 48 μmol; I_3^-: 47 μmol for NKX-2677). The molar amount of evolved H_2 exceeded the amount of the dye molecules contained in 50 mg of photocatalyst powder (NKX-2677: ca. 0.55 μmol; NKX-2697: ca. 0.52 μmol). The diffuse reflectance spectra for the NKX-2677-adsorbed photocatalysts after the reaction was found to be almost the same as before the reaction, except for a slight shift of the absorption edge to a shorter wavelength, as shown in Figure 43. This shift is attributable to the change in alignment of the dye molecules on the surface of the $Pt–H_4Nb_6O_{17}$ semiconductor during the stirring in the aqueous solution rather than to the decomposition of dye molecules, because a similar shift was also observed when the photocatalysts were stirred in an aqueous KI solution in the dark. The findings indicate that the following reactions took place over the NKX-2677 and NKX-2697 dye-adsorbed $Pt/H_4Nb_6O_{17}$ photocatalysts under visible light irradiation:

$$S + h\nu(\lambda > 400\,\text{nm}) \rightarrow S^* \text{ (excitation of dye)} \quad (11)$$

$$S^* \rightarrow S^+ + e^- \text{ (electron injection to } H_4Nb_6O_{17}) \quad (12)$$

$$e^- + H^+ \rightarrow 1/2\ H_2 \text{ (H_2 production on Pt)} \quad (13)$$

$$S^+ + I^- \rightarrow S + 1/2\ I_2 \text{ (1/2 } I_3^-) \text{ (regeneration of dye)} \quad (14)$$

On the other hand, the rate of H_2 production gradually decreased with irradiation time in the case of other coumarin dyes (C-343, NKX-2311, and NKX-2587), as shown in Figure 42b, while the rates of H_2 production were relatively high in initial period. The molar amount of liberated I_3^- was smaller than the amount of H_2 evolved in each case (e.g., H_2: 32 μmol; I_3^-: 25 μmol for NKX-2311). The diffuse reflectance spectra of these dyes changed significantly by the reaction, as shown in Figure 43. Such a significant change was not observed when the photocatalysts were stirred in the dark, indicating that the change in the spectra was caused by photochemical processes and not by physical processes such as desorption of dye molecules from the $Pt–H_4Nb_6O_{17}$ surface. It is likely that the oxidized state (S^+) of these dyes reacted with water before accepting an electron from the I^- anions and then became photo-inactive species.

5.3 Simultaneous Evolution of H_2 and O_2 under Visible Light Irradiation Using a Combination of Coumarin-Adsorbed $H_4Nb_6O_{17}$ and WO_3 Photocatalysts. As shown in Figure 44, the combination of NKX-2677-adsorbed $Pt–H_4Nb_6O_{17}$ and $IrO_2/Pt–WO_3$ resulted in simultaneous evolution of H_2 and O_2 in an almost stoichiometric ratio. The reaction proceeded without appreciable deactivation even after photoirradiation for 48 h. The total amount of evolved H_2 (ca. 116 μmol) exceeded the amount of dye molecules adsorbed on $Pt–H_4Nb_6O_{17}$ (ca. 0.55 μmol). On the other hand, the rate of gas evolution using NKX-2587 (which has one thiophene ring) decreased drastically with increasing irradiation time, as

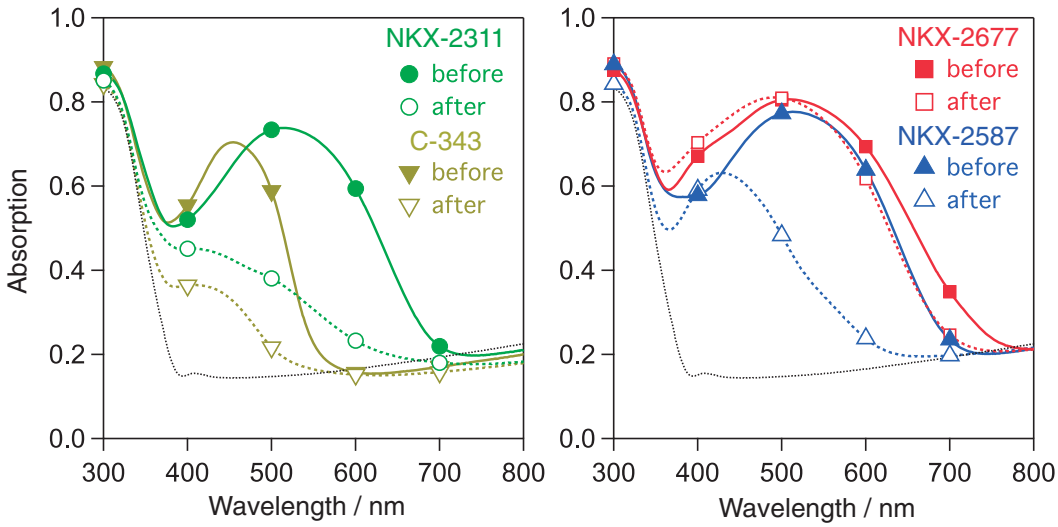

Figure 43. Diffuse reflectance spectra of coumarin dye-adsorbed $Pt/H_4Nb_6O_{17}$ photocatalysts before and after the reaction in Figure 42.

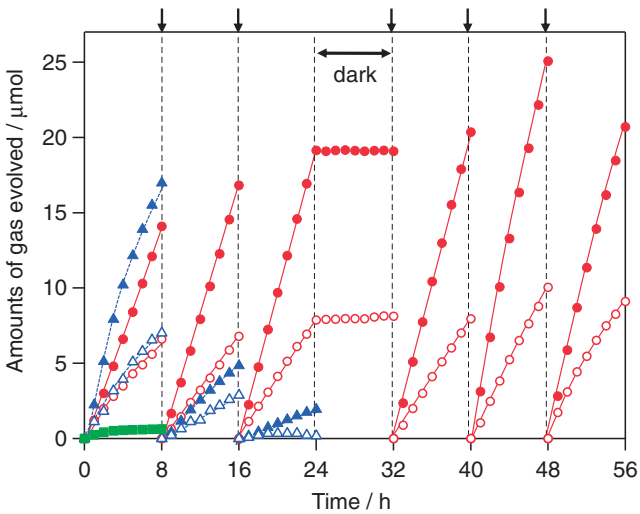

Figure 44. Time courses of photocatalytic evolution of H_2 (closed) and O_2 (open) using a mixture of coumarin dye-sensitized (circles: NKX-2677, triangles: NKX-2587, square: NKX-2311) $Pt/H_4Nb_6O_{17}$ (50 mg) and IrO_2–Pt/WO_3 (100 mg) suspended in a 5 mM of KI aqueous solution under visible light ($\lambda > 410$ nm). Allows indicate evacuation of gas phase.

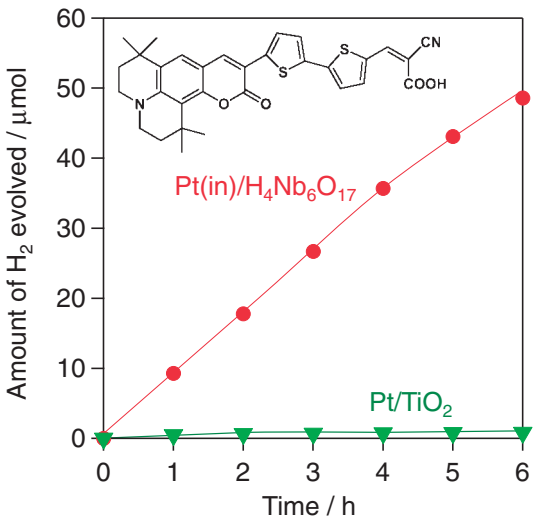

Figure 45. H_2 evolution over NKX-2677-adsorbed Pt(in)/$H_4Nb_6O_{17}$ and Pt/TiO_2 photocatalysts from aquous NaI (0.1 M) solution under visible light irradiation ($\lambda > 410$ nm).

Figure 44 shows. In the case of the NKX-2311 dye, which has no thiophene ring, only a small amount of H_2 was evolved during the initial period. These results again indicate that the oligothiophene moiety in coumarin dyes plays an essential role in stabilizing dye molecules during photocatalytic water splitting. Katoh et al. have examined the effect of light irradiation on the dyes adsorbed on nanocrystalline TiO_2 films under ambient conditions and found that dyes (not just coumarin dyes) containing an oligothiophene moiety are more stable than those without an oligothiophene moiety.[185] Transient absorption spectroscopy strongly implies that the positive charge in such dyes is located on the oligothiophene moiety. Therefore, the most likely explanation for the necessity of an oligothiophene moiety in the water-splitting reaction with I_3^-/I^- redox is that the positive charge of the oxidized dye is delocalized over the oligothiophene moiety reducing its reactivity toward H_2O, while it can accept an electron from an I^- anion thereby regenerating the original ground state of the dye.

"Nanostructured" reduction sites were successfully utilized in the dye-sensitized H_2 production system to control the reaction selectivity of electrons. As shown in Figure 45, H_2 evolution over NKX-2677-adsorbed Pt–TiO_2 terminated rapidly due to a significant backward reaction (reduction of I_3^- to I^-) on the Pt particles. On the other hand, H_2 evolution proceeded at a steady rate on NKX-2677-adsorbed Pt–$H_4Nb_6O_{17}$. This is a result of the backward reaction being suppressed by I_3^- anions being unable to access Pt particles because of the electrostatic repulsion between I_3^- and the negatively charged niobate layers (Figure 46).[109,110,112] Mallouk et al. first suggested this concept and demonstrated photocatalytic H_2 production over Ru-complex-adsorbed

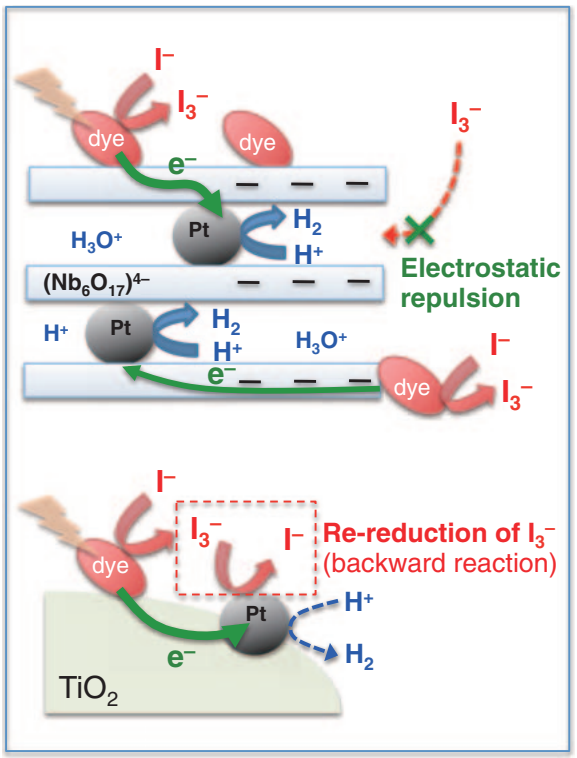

Figure 46. Conceptual scheme for suppression of backward reaction using nanostructured layered semiconductors.

Pt–$H_4Nb_6O_{17}$ in the presence of iodide electron donor.[109] Suppression of undesirable backward reactions with a redox mediator is critical for improving the overall efficiency in Z-scheme water-splitting systems. Although the affinity between photocatalyst materials and redox mediators has dominated the reaction selectivity in Z-scheme systems, introducing "nanostructured" reaction sites will allow the reactivity of electrons and holes to be controlled for the desired reactions, enabling efficient water splitting to be achieved under visible light.

5.4 Summary. Dye-sensitized overall water splitting under visible light irradiation was demonstrated for the first time using a simple organic dye molecule as a photosensitizer for H_2 evolution, WO_3 photocatalyst for O_2 evolution, and I_3^-/I^- redox couple as a shuttle redox mediator. The photocatalytic activity and electrochemical measurements indicated that the oxidized states of the coumarin dyes having oligothiophene moiety in their structure are stable even in water. It was first revealed that the unique stabilizing property of oligothiophene enabled one to achieve overall water splitting under visible light irradiation using such simple organic dye molecules as H_2-photocatalysts. This provides release from the difficulty in tuning the band levels of inorganic (particularly oxide) semiconductor photocatalysts, extending the diversity of photocatalysts for this Z-scheme water-splitting reaction. Although, the quantum efficiency of dye-sensitized H_2 evolution is currently low (e.g., <0.1% at 500 nm for the NKX-2677 system), the novel strategy of stabilizing positive charge in oligothiophene moieties of dye molecules promises efficient water splitting using structurally designed organic dye molecules.

6. Conclusion

A novel photocatalytic system that splits water into H_2 and O_2 was realized using a two-step photoexcitation system composed of a shuttle redox couple and two different semiconductor photocatalysts. We have first demonstrated water splitting based on the two-step photoexcitation process under UV light by using Pt-loaded anatase TiO_2 as the H_2 photocatalyst together with rutile TiO_2 for O_2 evolution in the presence of IO_3^-/I^- redox mediator. Although this system operates only under UV light ($\lambda < 400$ nm) due to the large band gap of the TiO_2 photocatalysts, it opened the way to achieve water splitting under visible light. The key was controlling the reactivity of electrons and holes with a redox mediator (IO_3^- and I^- anions) and water molecules. We have then achieved overall water splitting using various visible light responsive photocatalysts, such as $SrTiO_3$ doped with Cr, tantalum oxynitrides (TaON or $BaTaO_2N$), and organic dyes, which work as H_2 evolution photocatalysts, combined with tungsten oxide (WO_3) for O_2 evolution in the presence of a shuttle redox mediator such as iodate/iodide (IO_3^-/I^-) or triiodide/iodide (I_3^-/I^-). The use of $BaTaO_2N$ or coumarin organic dye was demonstrating to be photoactive at wavelengths up to ca. 660 nm. These results demonstrate the potential of a two-step water-splitting system for utilizing a broader band of visible spectrum.

Just 10 years ago, photocatalytic water splitting using a heterogeneous photocatalyst under visible light was considered a "dream reaction." However, water splitting under visible light has indeed been demonstrated in several heterogeneous photocatalytic systems over the last decade. The target quantum yield for splitting water into H_2 and O_2 is 30% at 600 nm, which corresponds to a solar energy conversion efficiency of about 5%. Although the introduction of Z-scheme water-splitting systems has significantly extended the available wavelengths (≈660 nm for H_2 evolution and ≈600 nm for O_2 evolution), the quantum efficiency (≈6%) is still too low to achieve this target. New strategies for achieving efficient separation of electrons and holes in powdered semiconductor photocatalysts are highly desirable. Another technical challenge is the construction of a system that can generate H_2 separately from O_2 to minimize the danger of explosions. The Z-scheme photocatalytic systems have the potential to be used in such separated water-splitting systems. Such an achievement will help solve global energy and environmental problems toward the realization of a sustainable society.

The author thanks Prof. Kazunari Domen, Prof. Hironori Arakawa, Prof. Bunsho Ohtani, and Dr. Kazuhiro Sayama for their support and encouragement. The author would like to express his deep appreciation to Dr. Kohjiro Hara, Dr. Masanobu Higashi, and Mr. Kenichi Shinmen for their collaborative work. These studies were supported by the Funding Program for Next Generation World-Leading Researchers (NEXT Program), also by JST PRESTO program, by the Fund for Young Researchers, and by the Research and Development in a New Interdisciplinary Field Based on Nanotechnology and Materials Science program of the Ministry of Education, Culture, Sports, Science and Technology, Japan.

References

1 A. Fujishima, K. Honda, *Nature* **1972**, *238*, 37.
2 J. R. Bolton, *Sol. Energy* **1996**, *57*, 37.
3 K. Domen, J. N. Kondo, M. Hara, T. Takata, *Bull. Chem. Soc. Jpn.* **2000**, *73*, 1307.
4 A. J. Esswein, D. G. Nocera, *Chem. Rev.* **2007**, *107*, 4022.
5 A. Kudo, Y. Miseki, *Chem. Soc. Rev.* **2009**, *38*, 253.
6 M. Kitano, M. Hara, *J. Mater. Chem.* **2010**, *20*, 627.
7 R. Abe, *J. Photochem. Photobiol., C* **2010**, *11*, 179.
8 S. Sato, J. M. White, *Chem. Phys. Lett.* **1980**, *72*, 83.
9 J.-M. Lehn, J.-P. Sauvage, R. Ziessel, *Nouv. J. Chim.* **1980**, *4*, 623.
10 K. Domen, S. Naito, M. Soma, T. Onishi, K. Tamaru, *J. Chem. Soc., Chem. Commun.* **1980**, 543.
11 K. Domen, S. Naito, T. Onishi, T. Tamaru, M. Soma, *J. Phys. Chem.* **1982**, *86*, 3657.
12 K. Domen, A. Kudo, T. Onishi, *J. Catal.* **1986**, *102*, 92.
13 K. Domen, A. Kudo, A. Shinozaki, A. Tanaka, K. Maruya, T. Onishi, *J. Chem. Soc., Chem. Commun.* **1986**, 356.
14 K. Domen, A. Kudo, M. Shibata, A. Tanaka, K. Maruya, T. Onishi, *J. Chem. Soc., Chem. Commun.* **1986**, 1706.
15 A. Kudo, A. Tanaka, K. Domen, T. Onishi, *J. Catal.* **1988**, *111*, 296.
16 A. Kudo, A. Tanaka, K. Domen, K. Maruya, K. Aika, T. Onishi, *J. Catal.* **1988**, *111*, 67.
17 A. Kudo, K. Sayama, A. Tanaka, K. Asakura, K. Domen, K. Maruya, T. Onishi, *J. Catal.* **1989**, *120*, 337.
18 K. Sayama, A. Tanaka, K. Domen, K. Maruya, T. Onishi, *Catal. Lett.* **1990**, *4*, 217.
19 Y. Inoue, T. Kubokawa, K. Sato, *J. Chem. Soc., Chem. Commun.* **1990**, 1298.
20 K. Sayama, A. Tanaka, K. Domen, K. Maruya, T. Onishi, *J. Phys. Chem.* **1991**, *95*, 1345.
21 Y. Inoue, T. Kubokawa, K. Sato, *J. Phys. Chem.* **1991**, *95*, 4059.
22 Y. Inoue, T. Niiyama, Y. Asai, K. Sato, *J. Chem. Soc., Chem. Commun.* **1992**, 579.
23 K. Sayama, H. Arakawa, *J. Phys. Chem.* **1993**, *97*, 531.
24 Y. Inoue, Y. Asai, K. Sato, *J. Chem. Soc., Faraday Trans.* **1994**, *90*, 797.
25 K. Sayama, H. Arakawa, *J. Photochem. Photobiol., A* **1994**, *77*, 243.
26 K. Sayama, H. Arakawa, K. Domen, *Catal. Today* **1996**, *28*, 175.
27 K. Sayama, H. Arakawa, *J. Chem. Soc., Faraday Trans.* **1997**, *93*, 1647.
28 T. Takata, Y. Furumi, K. Shinohara, A. Tanaka, M. Hara, J. N. Kondo, K. Domen, *Chem. Mater.* **1997**, *9*, 1063.
29 A. Kudo, H. Kato, *Chem. Lett.* **1997**, 867.
30 S. Ikeda, M. Hara, J. N. Kondo, K. Domen, H. Takahashi, T. Okubo, M. Kakihana, *Chem. Mater.* **1998**, *10*, 72.
31 H. Kato, A. Kudo, *Chem. Phys. Lett.* **1998**, *295*, 487.
32 H. G. Kim, D. W. Hwang, J. Kim, Y. G. Kim, J. S. Lee, *Chem. Commun.* **1999**, 1077.
33 C. Mitsui, H. Nishiguchi, K. Fukamachi, T. Ishihara, Y. Takita, *Chem. Lett.* **1999**, 1327.
34 H. Takahashi, M. Kakihana, Y. Yamashita, K. Yoshida, S. Ikeda, M. Hara, K. Domen, *J. Alloys Compd.* **1999**, *285*, 77.
35 H. Kato, A. Kudo, *Chem. Lett.* **1999**, 1207.
36 A. Kudo, H. Kato, *Chem. Phys. Lett.* **2000**, *331*, 373.
37 A. Kudo, H. Okutomi, H. Kato, *Chem. Lett.* **2000**, 1212.
38 A. Kudo, H. Kato, S. Nakagawa, *J. Phys. Chem. B* **2000**, *104*, 571.
39 M. Machida, S. Murakami, T. Kijima, S. Matsushima, M. Arai, *J. Phys. Chem. B* **2001**, *105*, 3289.
40 J. Sato, N. Saito, H. Nishiyama, Y. Inoue, *J. Phys. Chem. B* **2001**, *105*, 6061.
41 Z. Zou, J. Ye, K. Sayama, H. Arakawa, *Nature* **2001**, *414*, 625.
42 K. Ikarashi, J. Sato, H. Kobayashi, N. Saito, H. Nishiyama, Y. Inoue, *J. Phys. Chem. B* **2002**, *106*, 9048.
43 H. Kato, H. Kobayashi, A. Kudo, *J. Phys. Chem. B* **2002**, *106*, 12441.
44 Y.-G. Ko, W. Y. Lee, *Catal. Lett.* **2002**, *83*, 157.
45 V. R. Reddy, D. W. Hwang, J. S. Lee, *Catal. Lett.* **2003**, *90*, 39.
46 H. Kato, K. Asakura, A. Kudo, *J. Am. Chem. Soc.* **2003**, *125*, 3082.
47 J. Sato, H. Kobayashi, N. Saito, H. Nishiyama, Y. Inoue, *J. Photochem. Photobiol., A* **2003**, *158*, 139.
48 J. Sato, N. Saito, H. Nishiyama, Y. Inoue, *J. Phys. Chem. B* **2003**, *107*, 7965.
49 T. Ishihara, N. S. Baik, N. Ono, H. Nishiguchi, Y. Takita, *J. Photochem. Photobiol., A* **2004**, *167*, 149.
50 R. Abe, M. Higashi, Z. Zou, K. Sayama, Y. Abe, H. Arakawa, *J. Phys. Chem. B* **2004**, *108*, 811.
51 R. Abe, M. Higashi, Z. Zou, K. Sayama, Y. Abe, *Chem. Lett.* **2004**, *33*, 954.
52 J. N. Kondo, M. Uchida, K. Nakajima, L. Daling, M. Hara, K. Domen, *Chem. Mater.* **2004**, *16*, 4304.
53 A. Iwase, H. Kato, H. Okutomi, A. Kudo, *Chem. Lett.* **2004**, *33*, 1260.
54 J. Sato, H. Kobayashi, K. Ikarashi, N. Saito, H. Nishiyama, Y. Inoue, *J. Phys. Chem. B* **2004**, *108*, 4369.
55 T. Yanagida, Y. Sakata, H. Imamura, *Chem. Lett.* **2004**, *33*, 726.
56 J. Kim, D. W. Hwang, H. G. Kim, S. W. Bae, J. S. Lee, W. Li, S. H. Oh, *Top. Catal.* **2005**, *35*, 295.
57 Y. Ebina, N. Sakai, T. Sasaki, *J. Phys. Chem. B* **2005**, *109*, 17212.
58 Y. Miseki, H. Kato, A. Kudo, *Chem. Lett.* **2005**, *34*, 54.
59 H. Kadowaki, J. Sato, H. Kobayashi, N. Saito, H. Nishiyama, Y. Simodaira, Y. Inoue, *J. Phys. Chem. B* **2005**, *109*, 22995.
60 K. Shimizu, S. Itoh, T. Hatamachi, T. Kodama, M. Sato, K. Toda, *Chem. Mater.* **2005**, *17*, 5161.
61 K. Yoshioka, V. Petrykin, M. Kakihana, H. Kato, A. Kudo, *J. Catal.* **2005**, *232*, 102.
62 R. Abe, M. Higashi, K. Sayama, Y. Abe, H. Sugihara, *J. Phys. Chem. B* **2006**, *110*, 2219.
63 H. Jeong, T. Kim, D. Kim, K. Kim, *Int. J. Hydrogen Energy* **2006**, *31*, 1142.
64 Y. Miseki, H. Kato, A. Kudo, *Chem. Lett.* **2006**, *35*, 1052.
65 T. Kurihara, H. Okutomi, Y. Miseki, H. Kato, A. Kudo, *Chem. Lett.* **2006**, *35*, 274.
66 S. Ikeda, M. Fubuki, Y. K. Takahara, M. Matsumura, *Appl. Catal., A* **2006**, *300*, 186.
67 W. Yao, J. Ye, *Chem. Phys. Lett.* **2007**, *435*, 96.
68 H. Kadowaki, N. Saito, H. Nishiyama, Y. Inoue, *Chem. Lett.* **2007**, *36*, 440.
69 T. Mitsuyama, A. Tsutsumi, T. Hata, K. Ikeue, M. Machida, *Bull. Chem. Soc. Jpn.* **2008**, *81*, 401.
70 Y. Yuan, J. Zheng, X. Zhang, Z. Li, T. Yu, J. Ye, Z. Zou,

Solid State Ionics **2008**, *178*, 1711.
71 Y. Li, G. Chen, C. Zhou, Z. Li, *Catal. Lett.* **2008**, *123*, 80.
72 Y. Sakata, Y. Matsuda, T. Yanagida, K. Hirata, H. Imamura, K. Teramura, *Catal. Lett.* **2008**, *125*, 22.
73 H. Liu, J. Yuan, W. Shangguan, Y. Teraoka, *J. Phys. Chem. C* **2008**, *112*, 8521.
74 B. Sørensen, *Renewable Energy*, Academic Press, **1979**, p. 316.
75 K. Sayama, K. Mukasa, R. Abe, Y. Abe, H. Arakawa, *Chem. Commun.* **2001**, 2416.
76 K. Sayama, K. Mukasa, R. Abe, Y. Abe, H. Arakawa, *J. Photochem. Photobiol., A* **2002**, *148*, 71.
77 R. Abe, K. Sayama, H. Sugihara, *J. Phys. Chem. B* **2005**, *109*, 16052.
78 D. E. Scaife, *Sol. Energy* **1980**, *25*, 41.
79 J. R. Darwent, A. Mills, *J. Chem. Soc., Faraday Trans. 2* **1982**, *78*, 359.
80 W. Erbs, J. Desilvestro, E. Borgarello, M. Grätzel, *J. Phys. Chem.* **1984**, *88*, 4001.
81 K. Sayama, R. Yoshida, H. Kusama, K. Okabe, Y. Abe, H. Arakawa, *Chem. Phys. Lett.* **1997**, *277*, 387.
82 A. Kudo, K. Ueda, H. Kato, I. Mikami, *Catal. Lett.* **1998**, *53*, 229.
83 A. Kudo, K. Omori, H. Kato, *J. Am. Chem. Soc.* **1999**, *121*, 11459.
84 S. Tokunaga, H. Kato, A. Kudo, *Chem. Mater.* **2001**, *13*, 4624.
85 J. Yu, A. Kudo, *Adv. Funct. Mater.* **2006**, *16*, 2163.
86 M. Matsumura, Y. Saho, H. Tsubomura, *J. Phys. Chem.* **1983**, *87*, 3807.
87 A. Kudo, *Int. J. Hydrogen Energy* **2006**, *31*, 197.
88 A. Kudo, A. Nagane, I. Tsuji, H. Kato, *Chem. Lett.* **2002**, 882.
89 Z. Lei, W. You, M. Liu, G. Zhou, T. Takata, M. Hara, K. Domen, C. Li, *Chem. Commun.* **2003**, 2142.
90 N. Zheng, X. Bu, H. Vu, P. Feng, *Angew. Chem., Int. Ed.* **2005**, *44*, 5299.
91 D. Chen, J. Ye, *J. Phys. Chem. Solids* **2007**, *68*, 2317.
92 G. Hitoki, A. Ishikawa, T. Takata, J. N. Kondo, M. Hara, K. Domen, *Chem. Lett.* **2002**, 736.
93 Y. Lee, K. Nukumizu, T. Watanabe, T. Takata, M. Hara, M. Yoshimura, K. Domen, *Chem. Lett.* **2006**, *35*, 352.
94 N. Kakuta, K. H. Park, M. F. Finlayson, A. Ueno, A. J. Bard, A. Campion, M. A. Fox, S. E. Webber, J. M. White, *J. Phys. Chem.* **1985**, *89*, 732.
95 J. F. Reber, M. Rusek, *J. Phys. Chem.* **1986**, *90*, 824.
96 C. Xing, Y. Zhang, W. Yan, L. Guo, *Int. J. Hydrogen Energy* **2006**, *31*, 2018.
97 N. Bao, L. Shen, T. Takata, K. Domen, *Chem. Mater.* **2008**, *20*, 110.
98 H. Gerischer, *Photochem. Photobiol.* **1972**, *16*, 243.
99 J. Kiwi, M. Grätzel, *J. Am. Chem. Soc.* **1979**, *101*, 7214.
100 T. Kajiwara, K. Hashimoto, T. Kawai, T. Sakata, *J. Phys. Chem.* **1982**, *86*, 4516.
101 K. Hashimoto, T. Kawai, T. Sakata, *Nouv. J. Chim.* **1983**, *7*, 249.
102 H. Misawa, H. Sakuragi, Y. Usui, K. Tokumaru, *Chem. Lett.* **1983**, 1021.
103 T. Shimidzu, T. Iyoda, Y. Koide, *J. Am. Chem. Soc.* **1985**, *107*, 35.
104 A. W.-H. Mau, O. Johansen, W. H. F. Sasse, *Photochem. Photobiol.* **1985**, *41*, 503.
105 V. Heleg, I. Willner, *J. Chem. Soc., Chem. Commun.* **1994**, 2113.
106 E. A. Malinka, G. L. Kamalov, S. V. Vodzinskii, V. I. Melnik, Z. I. Zhilina, *J. Photochem. Photobiol., A* **1995**, *90*, 153.
107 R. Abe, K. Hara, K. Sayama, K. Domen, H. Arakawa, *J. Photochem. Photobiol., A* **2000**, *137*, 63.
108 K. Tennakone, J. Bandara, *Appl. Catal., A* **2001**, *208*, 335.
109 Y. I. Kim, S. J. Atherton, E. S. Brigham, T. E. Mallouk, *J. Phys. Chem.* **1993**, *97*, 11802.
110 G. B. Saupe, T. E. Mallouk, W. Kim, R. H. Schmehl, *J. Phys. Chem. B* **1997**, *101*, 2508.
111 R. Abe, K. Sayama, H. Arakawa, *Chem. Phys. Lett.* **2003**, *379*, 230.
112 R. Abe, K. Sayama, H. Arakawa, *J. Photochem. Photobiol., A* **2004**, *166*, 115.
113 R. Abe, K. Shinmei, K. Hara, B. Ohtani, *Chem. Commun.* **2009**, 3577.
114 M. Hara, C. C. Waraksa, J. T. Lean, B. A. Lewis, T. E. Mallouk, *J. Phys. Chem. A* **2000**, *104*, 5275.
115 W. J. Youngblood, S.-H. A. Lee, Y. Kobayashi, E. A. Hernandez-Pagan, P. G. Hoertz, T. A. Moore, A. L. Moore, D. Gust, T. E. Mallouk, *J. Am. Chem. Soc.* **2009**, *131*, 926.
116 R. Brimblecombe, A. Koo, G. C. Dismukes, G. F. Swiegers, L. Spiccia, *J. Am. Chem. Soc.* **2010**, *132*, 2892.
117 H. Kato, A. Kudo, *J. Phys. Chem. B* **2002**, *106*, 5029.
118 T. Ishii, H. Kato, A. Kudo, *J. Photochem. Photobiol., A* **2004**, *163*, 181.
119 R. Konta, T. Ishii, H. Kato, A. Kudo, *J. Phys. Chem. B* **2004**, *108*, 8992.
120 D. W. Hwang, H. G. Kim, J. S. Jang, S. W. Bae, S. M. Ji, J. S. Lee, *Catal. Today* **2004**, *93–95*, 845.
121 R. Niishiro, H. Kato, A. Kudo, *Phys. Chem. Chem. Phys.* **2005**, *7*, 2241.
122 D. W. Hwang, H. G. Kim, J. S. Lee, J. Kim, W. Li, S. H. Oh, *J. Phys. Chem. B* **2005**, *109*, 2093.
123 S. Nishimoto, M. Matsuda, M. Miyake, *Chem. Lett.* **2006**, *35*, 308.
124 R. Niishiro, R. Konta, H. Kato, W.-J. Chun, K. Asakura, A. Kudo, *J. Phys. Chem. C* **2007**, *111*, 17420.
125 Y. Shimodaira, H. Kato, H. Kobayashi, A. Kudo, *Bull. Chem. Soc. Jpn.* **2007**, *80*, 885.
126 T. Ikeda, T. Nomoto, K. Eda, Y. Mizutani, H. Kato, A. Kudo, H. Onishi, *J. Phys. Chem. C* **2008**, *112*, 1167.
127 J. Yoshimura, Y. Ebina, J. Kondo, K. Domen, A. Tanaka, *J. Phys. Chem.* **1993**, *97*, 1970.
128 H. G. Kim, D. W. Hwang, J. S. Lee, *J. Am. Chem. Soc.* **2004**, *126*, 8912.
129 S. Kohtani, N. Yamamoto, K. Kitajima, A. Kudo, H. Kato, K. Tokumura, K. Hayakawa, R. Nakagaki, *Photo/Electrochemistry & Photobiology in the Environment, Energy and Fuel*, **2004**, p. 173.
130 Y. Hosogi, Y. Shimodaira, H. Kato, H. Kobayashi, A. Kudo, *Chem. Mater.* **2008**, *20*, 1299.
131 Y. Hosogi, H. Kato, A. Kudo, *J. Mater. Chem.* **2008**, *18*, 647.
132 A. Kasahara, K. Nukumizu, G. Hitoki, T. Takata, J. N. Kondo, M. Hara, H. Kobayashi, K. Domen, *J. Phys. Chem. A* **2002**, *106*, 6750.
133 G. Hitoki, T. Takata, J. N. Kondo, M. Hara, H. Kobayashi, K. Domen, *Chem. Commun.* **2002**, 1698.
134 A. Kasahara, K. Nukumizu, T. Takata, J. N. Kondo, M. Hara, H. Kobayashi, K. Domen, *J. Phys. Chem. B* **2003**, *107*, 791.

135 M. Hara, J. Nunoshige, T. Takata, J. N. Kondo, K. Domen, *Chem. Commun.* **2003**, 3000.
136 D. Yamasita, T. Takata, M. Hara, J. N. Kondo, K. Domen, *Solid State Ionics* **2004**, *172*, 591.
137 M. Liu, W. You, Z. Lei, G. Zhou, J. Yang, G. Wu, G. Ma, G. Luan, T. Takata, M. Hara, K. Domen, C. Li, *Chem. Commun.* **2004**, 2192.
138 A. Ishikawa, T. Takata, J. N. Kondo, M. Hara, H. Kobayashi, K. Domen, *J. Am. Chem. Soc.* **2002**, *124*, 13547.
139 A. Ishikawa, Y. Yamada, T. Takata, J. N. Kondo, M. Hara, H. Kobayashi, K. Domen, *Chem. Mater.* **2003**, *15*, 4442.
140 A. Ishikawa, T. Takata, T. Matsumura, J. N. Kondo, M. Hara, H. Kobayashi, K. Domen, *J. Phys. Chem. B* **2004**, *108*, 2637.
141 K. Ogisu, A. Ishikawa, K. Teramura, K. Toda, M. Hara, K. Domen, *Chem. Lett.* **2007**, *36*, 854.
142 K. Maeda, T. Takata, M. Hara, N. Saito, Y. Inoue, H. Kobayashi, K. Domen, *J. Am. Chem. Soc.* **2005**, *127*, 8286.
143 K. Maeda, K. Teramura, D. Lu, T. Takata, N. Saito, Y. Inoue, K. Domen, *Nature* **2006**, *440*, 295.
144 Y. Lee, H. Terashima, Y. Shimodaira, K. Teramura, M. Hara, H. Kobayashi, K. Domen, M. Yashima, *J. Phys. Chem. C* **2007**, *111*, 1042.
145 I. Tsuji, H. Kato, A. Kudo, *Angew. Chem., Int. Ed.* **2005**, *44*, 3565.
146 G. Li, T. Kako, D. Wang, Z. Zou, J. Ye, *J. Solid State Chem.* **2007**, *180*, 2845.
147 H. Irie, Y. Maruyama, K. Hashimoto, *J. Phys. Chem. C* **2007**, *111*, 1847.
148 R. Abe, K. Sayama, K. Domen, H. Arakawa, *Chem. Phys. Lett.* **2001**, *344*, 339.
149 H. Kato, M. Hori, R. Konta, Y. Shimodaira, A. Kudo, *Chem. Lett.* **2004**, *33*, 1348.
150 R. Abe, T. Takata, H. Sugihara, K. Domen, *Chem. Commun.* **2005**, 3829.
151 H. Kato, Y. Sasaki, A. Iwase, A. Kudo, *Bull. Chem. Soc. Jpn.* **2007**, *80*, 2457.
152 Y. Sasaki, A. Iwase, H. Kato, A. Kudo, *J. Catal.* **2008**, *259*, 133.
153 M. Higashi, R. Abe, A. Ishikawa, T. Takata, B. Ohtani, K. Domen, *Chem. Lett.* **2008**, *37*, 138.
154 M. Higashi, R. Abe, K. Teramura, T. Takata, B. Ohtani, K. Domen, *Chem. Phys. Lett.* **2008**, *452*, 120.
155 M. Higashi, R. Abe, T. Takata, K. Domen, *Chem. Mater.* **2009**, *21*, 1543.
156 Y. Sasaki, H. Nemoto, K. Saito, A. Kudo, *J. Phys. Chem. C* **2009**, *113*, 17536.
157 M. Tabata, K. Maeda, M. Higashi, D. Lu, T. Takata, R. Abe, K. Domen, *Langmuir* **2010**, *26*, 9161.
158 K. Maeda, M. Higashi, D. Lu, R. Abe, K. Domen, *J. Am. Chem. Soc.* **2010**, *132*, 5858.
159 R. Abe, M. Higashi, K. Domen, *ChemSusChem* **2011**, *4*, 228.
160 K. Maeda, R. Abe, K. Domen, *J. Phys. Chem. C* **2011**, *115*, 3057.
161 A. J. Bard, *J. Photochem.* **1979**, *10*, 59.
162 K. Tennakone, S. Pushpa, *J. Chem. Soc., Chem. Commun.* **1985**, 1435.
163 K. Tennakone, S. Wickramanayake, *J. Chem. Soc., Faraday Trans. 2* **1986**, *82*, 1475.
164 K. Tennakone, R. Tantrigoda, S. Abeysinghe, S. Punchihewa, C. A. N. Fernando, *J. Photochem. Photobiol., A* **1990**, *52*, 43.
165 T. Ohno, S. Saito, K. Fujihara, M. Matsumura, *Bull. Chem. Soc. Jpn.* **1996**, *69*, 3059.
166 T. Ohno, K. Fujihara, S. Saito, M. Matsumura, *Sol. Energy Mater. Sol. Cells* **1997**, *45*, 169.
167 T. Ohno, D. Haga, K. Fujihara, K. Kaizaki, M. Matsumura, *J. Phys. Chem. B* **1997**, *101*, 6415.
168 T. Ohno, K. Nakabeya, K. Fujihara, M. Matsumura, *J. Photochem. Photobiol., A* **1998**, *117*, 143.
169 K. Fujihara, T. Ohno, M. Matsumura, *J. Chem. Soc., Faraday Trans.* **1998**, *94*, 3705.
170 T. Ohno, K. Fujihara, K. Sarukawa, M. Matsumura, *Z. Phys. Chem.* **1999**, *213*, 165.
171 G. R. Bamwenda, K. Sayama, H. Arakawa, *J. Photochem. Photobiol., A* **1999**, *122*, 175.
172 R. Abe, K. Sayama, H. Arakawa, *Chem. Phys. Lett.* **2003**, *371*, 360.
173 A. Tsujiko, T. Kisumi, Y. Magari, K. Murakoshi, Y. Nakato, *J. Phys. Chem. B* **2000**, *104*, 4873.
174 T. Ohno, K. Sarukawa, M. Matsumura, *New J. Chem.* **2002**, *26*, 1167.
175 S.-C. Moon, H. Mametsuka, S. Tabata, E. Suzuki, *Catal. Today* **2000**, *58*, 125.
176 G. M. Berry, B. G. Bravo, M. E. Bothwell, G. J. Cali, J. E. Harris, T. Mebrahtu, S. L. Michelhaugh, J. F. Rodriguez, M. P. Soriaga, *Langmuir* **1989**, *5*, 707.
177 R. Abe, H. Takami, N. Murakami, B. Ohtani, *J. Am. Chem. Soc.* **2008**, *130*, 7780.
178 M. Sadakane, K. Sasaki, H. Kunioku, B. Ohtani, W. Ueda, R. Abe, *Chem. Commun.* **2008**, 6552.
179 W.-J. Chun, A. Ishikawa, H. Fujisawa, T. Takata, J. N. Kondo, M. Hara, M. Kawai, Y. Matsumoto, K. Domen, *J. Phys. Chem. B* **2003**, *107*, 1798.
180 R. Abe, M. Higashi, K. Domen, *J. Am. Chem. Soc.* **2010**, *132*, 11828.
181 B. O'Regan, M. Grätzel, *Nature* **1991**, *353*, 737.
182 K. Hara, Z.-S. Wang, T. Sato, A. Furube, R. Katoh, H. Sugihara, Y. Dan-oh, C. Kasada, A. Shinpo, S. Suga, *J. Phys. Chem. B* **2005**, *109*, 15476.
183 D. P. Hagberg, T. Marinado, K. M. Karlsson, K. Nonomura, P. Qin, G. Boschloo, T. Brinck, A. Hagfeldt, L. Sun, *J. Org. Chem.* **2007**, *72*, 9550.
184 T. A. Heimer, S. T. D'Arcangelis, F. Farzad, J. M. Stipkala, G. J. Meyer, *Inorg. Chem.* **1996**, *35*, 5319.
185 R. Katoh, A. Furube, S. Mori, M. Miyashita, K. Sunahara, N. Koumura, K. Hara, *Energy Environ. Sci.* **2009**, *2*, 542.

Ryu Abe received his B.S. (1996), M.S. (1998), and Ph.D. (2001) degrees from Tokyo Institute of Technology. He then worked as a postdoctoral fellow (2001–2002) and as a researcher (2002–2005) at the National Institute of Advanced Industrial Science and Technology (AIST), Japan. In 2005, his academic career as an Associate Professor began at the Catalysis Research Center, Hokkaido University. His research is mainly focused on the development of new photocatalysts for water splitting and environmental purification.